CAPITAL UNIVERSITY OF SCIENCE AND TECHNOLOGY, ISLAMABAD

Numerical Analysis of Radiation Effects on the Flow and Heat Transfer within a Lid-Driven Square Cavity through Porous Medium

by

Maryam Bibi

A thesis submitted in partial fulfillment for the degree of Master of Philosophy

in the

Faculty of Computing
Department of Mathematics

2025

CERTIFICATE OF APPROVAL

Numerical Analysis of Radiation Effects on the Flow and Heat Transfer within a Lid-Driven Square Cavity through Porous Medium

by

Maryam Bibi

(MMT223007)

THESIS EXAMINING COMMITTEE

S. No.	Examiner	Name	Organization
(a)	External Examiner	Dr. Shahzad Munir	CU, Islamabad
(b)	Internal Examiner	Dr. Dur-e-Shehwar	CUST, Islamabad

Dr. Muhammad Sabeel Khan
Thesis Supervisor
November , 2025

Dr Muhammad Sagheer
Head
Dept. of Mathematics
November , 2025

Dr M. Abdul Qadir
Dean
Faculty of Computing
November , 2025

Author's Declaration

I, **Maryam Bibi**, hereby state that my MS thesis titled **"Numerical Analysis of Radiation Effects on the Flow and Heat Transfer within a Lid-Driven Square Cavity through Porous Medium"** work and has not been submitted previously by me for taking any degree from Capital University of Science and Technology, Islamabad or anywhere else in the country/abroad.

At any time if my statement is found to be incorrect even after my graduation, the University has the right to withdraw my M.Phil Degree.

(Maryam Bibi)

Registration No. MMT223007

Plagiarism Undertaking

I solemnly declare that research work presented in this thesis titled **"Numerical Analysis of Radiation Effects on a Flow and Heat Transfer within a Lid-Driven Cavity through Porous Medium"** is solely my research work with no significant contribution from any other person. Small contribution/help wherever taken has been duly acknowledged and that complete thesis has been written by me.

I understand the zero tolerance policy of the HEC and Capital University of Science and Technology towards plagiarism. Therefore, I as an author of the above titled thesis declare that no portion of my thesis has been plagiarized and any material used as reference is properly referred/cited.

I undertake that if I am found guilty of any formal plagiarism in the above titled thesis even after award of M.Phil Degree, the University reserves the right to withdraw/revoke my M.Phil degree and that HEC and the University have the right to publish my name on the HEC/University website on which names of students are placed who submitted plagiarized work.

(Maryam Bibi)
Registration No. MMT223007

Acknowledgement

In the name of **ALLAH**, the Most Gracious and Merciful, who blessed humanity with the wisdom and knowledge to explore the mysteries of the universe after bringing it into existence. First and foremost, I would like to express my deepest gratitude to my supervisor, **Dr. Muhammad Sabeel Khan**, for their continuous support, patience, and invaluable guidance throughout the course of this research. Their expertise and encouragement have been instrumental in the completion of this thesis.

I would like to express my deepest gratitude to my parents, whose unconditional love, constant support, and unwavering belief in me have been the foundation of my academic journey. Their sacrifices, encouragement, and guidance have shaped who I am today and have given me the strength to pursue my goals. Thank you for always standing by me, for believing in my dreams, and for being my greatest source of motivation. This thesis is as much yours as it is mine.

I am also sincerely grateful to my fellow researchers for their constructive feedback and insightful suggestions, which greatly enriched the quality of my work.

Lastly, I would like to thank my family and friends for their unwavering support and encouragement throughout this journey. Their belief in me gave me strength during challenging times. A special thanks goes to my dear husband **Hussain Abbasi**, who support me to achieve my target.

(Maryam Bibi)
Registration No: MMT223007

Abstract

This thesis presents a comprehensive numerical investigation of Darcy–Forchheimer flow with radiative heat transfer in a lid-driven square cavity using the Finite Element Method implemented in `FreeFEM++`. The governing equations consist of coupled, partial differential equations representing continuity, momentum, and energy conservation, incorporating porous medium effects through the Darcy and Forchheimer parameters, along with thermal transport effects governed by the Prandtl and radiation parameters. The upper lid of the cavity moves with a uniform velocity, inducing forced convection, while the bottom wall is heated and the top wall is cooled, leading to a combined convective and radiative heat transfer phenomenon. The computational methodology employs an unstructured mesh with FEM-based spatial discretizations. Extensive simulations are performed to analyze the combined influence of Reynold number, Grashhof number, Prandtl number, and thermal radiation on the flow structure and thermal behavior. The results reveal that at low Reynolds number, viscous forces dominate, resulting in smooth circulation and symmetric vortex structures. With increasing Reynolds number, inertial effects become significant, shifting the primary vortex toward the upper-left corner and forming secondary vortices near the walls. For small Prandtl number (e.g., liquid metals), thermal diffusion dominates, giving nearly uniform temperature fields, whereas larger Prandtl number leads to thinner thermal boundary layers and stronger temperature stratification. The radiation parameter thermal radiation enhances heat transfer near the walls; low thermal radiation yields smooth isotherms, while high thermal radiation produces steeper gradients and compressed thermal layers. Reducing Grashhof number (higher permeability) strengthens convection and vortex intensity, whereas Grashhof number has a minor effect at low Reynolds number but becomes more influential at higher Reynolds number. The findings provide valuable physical insights into complex transport phenomena in porous cavities with radiative effects. These results have potential applications in energy systems, heat exchangers, and thermal management in porous enclosures.

Contents

List of Figures

List of Tables

Abbreviations

CFD	Computational Fluid Dynamics
FEM	Finite Element Method
FVM	Finite Volume Method
GFEM	Galerkin Finite Element Method
NSD	Navier-Stokes/Darcy Model
NSF	Navier-Stokes/Forchheimer Model
NEN	Total Number of Finite Elements
PDE	Partial Differential Equation

Symbols

P	Pressure
A	Area
t	Time
∇	Gradient operator
Δ	Laplace operator
ρ	Density
μ	Dynamic viscosity
u_o, v_o	Characteristics velocity
V_h, U_h	Approximation functions
$\tilde{U}, \tilde{V}$	Test functions
L	Characteristics length
k	Thermal conductivity
α, β	Constant
p_v	Viscous resistance
p_i	Inertial resistance
λ	Porosity parameter
h	Length of each finite element sub-interval
ϕ_i	Basis functions
Pr	Prandtl number
Re	Reynolds number
R_d	Thermal radiation
Gr	Grashhof number
C_p	Specific heat constant

W	Velocity-approximating finite element spaces
Q	Pressure-approximating finite element spaces
Ω	Computational domain
$\tilde{t}$	Variation of time
$\tilde{T}$	Variation of temperature
T_∞	Ambient temperature
σ	Electrical conductivity
ϕ, ψ	Scalar functions
ξ_j	Shape functions
ν	Kinematic viscosity
μ	Dynamic viscosity
q_r	Radiative heat flux

Chapter 1

Introduction and Literature Survey

The study of fluid flow through porous media has received significant attention due to its applications in geothermal systems, oil and gas extraction, groundwater movement, thermal insulation, biomedical fluid transport, and energy storage technologies [1, 2]. In porous materials, the interaction between a saturating fluid and the solid matrix gives rise to complex flow behavior that cannot be accurately described by classical fluid dynamics. Early investigations relied on Darcy's law—a linear model proposed for low-velocity flows in homogeneous porous structures [3]. However, its validity is limited to creeping flows and fails to capture inertial effects. To address these limitations, the Darcy–Forchheimer model was introduced, incorporating a nonlinear drag term to represent resistance in denser or more complex porous media [4, 5]. This model is essential for simulating high-velocity porous flows in practical applications such as packed-bed reactors and catalytic converters. Flow behavior is affected by porosity gradients, anisotropy, and heterogeneity. Whitaker [6] developed the volume averaging technique to link micro- and macroscopic scales, leading to macroscopic equations from the Navier–Stokes framework. Vafai and Kaviany emphasized the importance of thermal dispersion and local thermal non-equilibrium effects, especially under strong thermal gradients or internal heat generation. Foundational work by Horton and

Rogers [7], Lapwood [8], and Wooding [9] established the criteria for buoyancy-driven convection and thermal instability in porous layers. These insights have been expanded in modern research, incorporating multiphysics coupling involving heat transfer, radiation, magnetic effects, and chemical reactions [10]. Models now include variable porosity, compressibility, non-Newtonian behavior, and electromagnetic fields, leading to complex simulations using numerical tools like the Finite Element Method (FEM).

The Darcy–Forchheimer model extends the classical Darcy's law by incorporating both viscous and inertial effects, making it particularly suitable for moderate to high-velocity flows in porous media. While Darcy's law is applicable for slow-moving fluids where inertial forces are negligible, it fails to capture nonlinear momentum transport phenomena encountered in practical applications such as filtration, petroleum recovery, packed-bed reactors, and electronic cooling systems [2, 3].

The Forchheimer correction introduces a quadratic velocity term to account for drag caused by fluid–solid interactions within the porous structure. This correction is essential in accurately predicting momentum and heat transfer behavior, especially in regimes where inertial effects are non-negligible [11, 12].

Ignoring this nonlinear term often results in significant underprediction of temperature gradients, Nusselt number, and overall heat fluxes in mixed convection or forced convection scenarios involving high permeability porous layers [13, 14]. Recent studies have extensively applied the Darcy–Forchheimer model in simulations of radiative–convective flows through porous enclosures and cavities.

These include investigations into thermal boundary layer behavior, entropy generation, and buoyancy-assisted heat transfer enhancement [15, 16]. The model's capacity to handle the combined effects of inertia, porosity, and thermal radiation makes it a key framework for modern porous media heat transfer analysis. Heat transfer in porous media encompasses conduction, convection, and sometimes radiation, depending on the medium's properties and the saturating fluid [2]. This is evident in systems like geothermal reservoirs, biological tissues, insulation

materials, and packed-bed reactors. The local thermal non-equilibrium model becomes necessary, where separate energy equations are solved for the fluid and solid phases [5].

Several studies confirm that assuming local thermal equilibrium can result in inaccuracies, particularly under forced convection or radiation. Thermal dispersion—arising from microscopic velocity fluctuations—also plays a key role in enhancing effective thermal conductivity.

Vafai and Tien [2] analyzed the influence of boundary and inertia effects on forced convection, showing that neglecting these effects may underpredict heat transfer. In high-speed flows such as filtration and industrial drying, the Darcy–Forchheimer model becomes essential [3].

Natural convection in porous enclosures is primarily driven by the Rayleigh number, permeability, and porosity, with lower critical Rayleigh numbers in porous media compared to simple fluids. Advanced models incorporate additional mechanisms such as viscous dissipation, radiative heat transfer, and internal heat generation [17]. Ingham and Pop [18] explored these mechanisms, including anisotropic conduction and variable thermal properties.

Vafai [2] also highlighted temperature dependent thermal conductivity and specific heat in modeling high-temperature porous systems. Finite element and finite volume techniques are frequently used to solve the coupled energy and momentum equations, enabling accurate simulations of complex heat transfer behavior in porous domains. Thermal radiation is crucial in high-temperature porous systems such as combustion chambers, packed-bed reactors, solar receivers, and re-entry shields [2, 3]. When temperature differences are significant or when pores are semitransparent, radiative heat transfer contributes substantially to the thermal balance. To incorporate radiative effects, the Rosseland diffusion approximation is often employed, which simplifies the radiative heat flux as a function of the temperature gradient under the assumption of optically thick media [17]. El-Aziz [19] demonstrated that radiation enhances the heat transfer rate in porous boundary-layer flows, increasing surface temperatures and thinning thermal boundary layers.

In chemically reactive or multiphase porous flows, thermal radiation affects not just heat transfer, but also mass transport and reaction rates, particularly in the presence of heat generation. Accurate modeling of radiation requires temperature-dependent thermophysical properties such as emissivity, absorptivity, and radiative conductivity. Numerical simulations of radiative-convective flows necessitate fine meshes and robust solvers due to strong nonlinearity.

FEM and other methods have proven effective in simulating such systems, including porous fins, nanofluid-filled cavities, and radiative insulation layers. The FEM is a powerful numerical tool for modeling heat and momentum transport in porous systems, especially when radiation effects are included. FEM offers high adaptability to complex geometries, anisotropic properties, and mixed boundary conditions [20].

In porous media, FEM discretizes governing equations from Brinkman models, as well as the energy equation with conduction, convection, and radiation. Nonlinear radiative terms, such as those arising from temperature-dependent emissivity, can be efficiently handled using variational formulations [21].

The mesh adaptability in FEMallows focused resolution of steep gradients near walls or porous–fluid interfaces, making it superior to finite difference or control volume approaches for porous media applications. FEM has been successfully applied to simulate radiative–convective heat transfer in porous enclosures, where analytical solutions are infeasible.

FreeFem++ has emerged as a powerful open-source FEM software for solving coupled nonlinear problems [22]. As a result, accurate modeling of flow through porous media remains a critical research area with emphasis on thermal–fluid–structural interactions.

1.1 Thesis Contribution

The main contributions of this thesis can be summarized as follows.

Understanding and analyzing a comprehensive mathematical model for Darcy–Forchheimer flow with radiative heat transfer inside a lid-driven square cavity. The model incorporates the combined effects of the Darcy-Forchheimer parameters, Prandtl number, and radiation parameter on the fluid flow and heat transfer characteristics.

Developing a Finite Element Method (FEM) framework and coding it in `FreeFEM++` to solve the coupled partial differential equations governing the velocity, pressure, and temperature fields.

Performing an extensive parametric study to investigate the combined influence of Gr_v, Gr_i, Pr, and Rd on flow dynamics and thermal behavior. The results reveal significant effects of porous resistance, inertial forces, and radiative heat transfer on velocity distribution and temperature field.

1.2 Thesis Layout

This thesis is further composed of the following chapters:

1.2.1 Chapter 2

demonstrates the introductory basics of fluid dynamics. A brief discussion about the basic definitions, governing laws for fluid motion and governing equations have been illustrated. Dimensionless physical quantities of interest are also mentioned briefly related to the problems.

1.2.2 Chapter 3

In Chapter 3, the finite element method has been explained by taking examples in one-dimensional and two-dimensional problem . The problem are solved to explain the numerical procedure for the calculation of the solutions.

1.2.3 Chapter 4

In chapter 4 the effects of thermal radiation on the fluid flow through a porous medium are analyzed using the FEM based on the Galerkin weighted residual approach. The governing dimensional equations are first non-dimensionalized through suitable transformations, and appropriate boundary conditions are incorporated. The partial differential equations (PDEs) are then converted from their strong form to the weak form by multiplying each equation by corresponding test functions from the same function space and integrating over the entire computational domain. An approximate solution is subsequently obtained by employing a set of trial (basis) functions defined locally over finite elements within the domain. This methodology enables accurate numerical simulation of the coupled transport phenomena in porous media under radiative effects. Results are presented in the form of graphs, isotherms and streamlines.

1.2.4 Chapter 5

Chapter 5 Contains the conclusion of this work and some future direction are shown.

Chapter 2

Fundamental Concepts in Fluid Mechanics

In this chapter we are going to discuss some basic concepts, definitions and governing laws related to the fluid dynamics. Dimensionless quantities are also discussed which appears in the presented mathematical subsequent chapters.

2.1 Basic Definitions

Some of the basic definitions are given bellow:

2.1.1 Physical Properties of the Fluid

2.1.1.1 Mass Density or Density

"Density or Mass Density of a fluid is defined as the ratio of the mass of a fluid to its volume. Thus mass per unit volume of a fluid is called density. It is denoted by ρ. The unit of mass density in SI unit is Kg per cubic meter, i.e., Kg/m^3. Mathematically, mass density is written as:

$$\rho = \frac{\text{Mass of fluid}}{\text{Volume of fluid}}.$$

The value of density of water is 1 gm/cm^3 or 1000 kg/m^3." [23]

2.1.1.2 Pressure

"When a fluid is contained in a vessel, it exerts force at all points on the sides and bottom and top of the container. The force per unit area is called pressure. If, P represents the force, and A is the area on which the force acts; then intensity of pressure,

$$p = \frac{P}{A}.$$

The pressure of a fluid on a surface will always act normal to the surface." [24]

2.1.1.3 Viscosity

"Viscosity is defined as the property of a fluid which offers resistance to the movement of one layer of fluid over another adjacent layer of the fluid. When two layers of a fluid, a distance apart, move one over the other at different velocities, say u and $u+du$, the viscosity together with relative velocity causes a shear stress acting between the fluid layers. The top layer causes a shear stress on the adjacent lower layer while the lower layer causes a shear stress on the adjacent top layer. This shear stress is proportional to the rate of change of velocity with respect to y. It is denoted by symbol τ (Tau).

Mathematically,

$$\tau \propto \frac{du}{dy}$$

or

$$\tau = \mu \frac{du}{dy}$$

where, μ (called mu) is the constant of proportionality and is known as the coefficient of dynamic viscosity or only viscosity." [23]

2.1.1.4 Kinematic Viscosity

"It is defined as the ratio between the dynamic viscosity and density of fluid. It is denoted by symbol ν read as **"nu"**.
Mathematically,

$$\nu = \frac{\mu}{\rho}." \text{ [24]}$$

2.1.1.5 Thermal Conductivity

"The Fourier heat conduction law states that the heat flow is proportional to the temperature gradient. The coefficient of proportionality is a material parameter known as the thermal conductivity, which may be a function of several variables." [25]

2.2 Dimensionless Parameters

The following dimensionless numbers will appear in the discussion given in the next chapters.

2.2.1 Prandtl Number

"This number expresses the ratio of the momentum diffusivity (viscosity) to the thermal diffusivity. It characterizes the physical properties of a fluid with convective and diffusive heat transfers. It describes, for example, the phenomena connected with the energy transfer in a boundary layer. It expresses the degree of similarity between velocity and diffusive thermal fields or, alternatively, between hydrodynamic and thermal boundary layers. With $Pr = 1$ and grad $p = 0$, the thermal and hydrodynamic fields are similar. For example, if diverse molten materials have equal Prandtl numbers, they have similar velocity and temperature fields in crystallization.

$$Pr = \frac{\eta c_p}{\lambda},$$

where, η represents the dynamic viscosity, c_p denotes the specific heat capacity and λ stands for thermal conductivity." [26]

2.2.2 Reynolds Number

$$Re = \frac{wL}{\nu},$$

"where, w represents the characteristic velocity of the fluid, L denotes the characteristic length of the system, is the kinematic viscosity of the fluid.

This number expresses the ratio of the fluid inertia force to that of molecular friction (viscosity). It characterizes the hydrodynamic conditions for viscous fluid flow.

It determines the character of the flow (laminar, turbulent and transient flows). For a laminar flow $Re < 2000$ is valid, for a transient flow $2000 < Re < 4000$, and for a turbulent flow it is $Re > 4000$.

With low values of the Re number, the viscous friction muffles the originating dynamic influence of the flow relatively quickly and intensively, due to which the streamlines and elementary fluid volumes cannot be deformed substantially and the flow remains laminar.

With large Re numbers, the dynamic flow effect cannot be equalized by viscous friction and the flow stability is lost, which is manifested by swirls and turbulence in the fluid." [26]

2.2.3 Grashof Number

$$Gr = \frac{L^3 g \beta \Delta T}{\nu^2}$$

where L represents the characteristic length of the system, g denotes the acceleration due to gravity, β is the coefficient of thermal expansion of the fluid, ΔT

indicates the temperature difference between the heated surface and the surrounding fluid, and ν is the kinematic viscosity of the fluid.

The Grashof Number expresses the ratio of the product of inertia and buoyancy forces to the square of a viscous force. It characterizes the mass transfer by natural convection in a non-isotropic vapour gas mixture, with the transfer being caused by the temperature difference and vapour concentration in the air of the vapour gas mixture [26].

2.3 Types of Fluid Flow

2.3.1 Steady and Unsteady Flows

2.3.1.1 Steady Flow

"The type of flow in which the fluid characteristics like velocity, pressure, density, etc. at a point do not change with time is called steady flow. Mathematically, we have:

$$\left(\frac{\partial u}{\partial t}\right)_{x_0,y_0,z_0} = 0; \left(\frac{\partial v}{\partial t}\right)_{x_0,y_0,z_0} = 0; \left(\frac{\partial w}{\partial t}\right)_{x_0,y_0,z_0} = 0;$$

$$\left(\frac{\partial p}{\partial t}\right)_{x_0,y_0,z_0} = 0; \left(\frac{\partial \rho}{\partial t}\right)_{x_0,y_0,z_0} = 0; \quad \text{and so on.}$$

Where (x_0, y_0, z_0) is a fixed point in a fluid field where these variables are being measured w.r.t. time." [24].

Example: Flow through a prismatic or non-prismatic conduit at a constant flow rate Qm^3/s is steady. (A prismatic conduit has a constant size shape and has a velocity equation in the form $u = ax^2 + bx + c$, which is independent of time t).

2.3.1.2 Unsteady Flow

"It is that type of flow in which the velocity, pressure or density at a point change w.r.t. time.

Mathematically, we have:

$$\left(\frac{\partial u}{\partial t}\right)_{x_0,y_0,z_0} \neq 0; \left(\frac{\partial v}{\partial t}\right)_{x_0,y_0,z_0} \neq 0; \left(\frac{\partial w}{\partial t}\right)_{x_0,y_0,z_0} \neq 0;$$

$$\left(\frac{\partial p}{\partial t}\right)_{x_0,y_0,z_0} \neq 0; \left(\frac{\partial \rho}{\partial t}\right)_{x_0,y_0,z_0} \neq 0 \text{ and so on.}$$

Example:
The flow in a pipe whose valve is being opened or closed gradually (velocity equation is in the form $u(x,t) = ax^2 + bxt$)". [24]

2.3.2 One, Two and Three Dimensional Flows

2.3.3 One Dimensional Flow

"It is that type of flow in which the flow parameter such as velocity is a function of time and one space co-ordinate only.

Mathematically:

$$u = f(x),$$

$$v = 0, \quad w = 0.$$

where u, v and w are velocity components in x, y and z directions respectively.

Example: Flow in a pipe where average flow parameters are considered for analysis." [24]

2.3.4 Two Dimensional Flow

"The flow in which the velocity is a function of time and two rectangular space coordinates is called two dimensional flow.

Mathematically:

$$u = f_1(t, x, y),$$

$$u = f_2(t, x, y),$$

$$w = 0.$$

Examples:

(i) Flow between parallel plates of infinite extent. (ii) Flow in the main stream of a wide river." [24]

2.3.5 Three Dimensional Flow

"It is that type of flow in which the velocity is a function of time and three mutually perpendicular directions. Mathematically:

$$u = f_1(t, x, y, z),$$

$$v = f_2(t, x, y, z),$$

$$w = f_3(t, x, y, z).$$

Examples:

(i) Flow in a converging or diverging pipe or channel.

(ii) Flow in a prismatic open channel in which the width and the water depth are of the same order of magnitude." [24]

2.3.6 Laminar and Turbulent Flows

2.3.6.1 Laminar Flow

"A laminar flow is one in which paths taken by the individual particles do not cross one another and move along well defined paths.
Examples:

(i) Flow through a capillary tube.

(ii) Flow of blood in veins and arteries.

(iii) Ground water flow." [24]

2.3.6.2 Turbulent Flow

"A turbulent flow is that flow in which fluid particles move in a zig zag way.

Example: High velocity flow in a conduit of large size. The majority of fluid flow issues that arise in engineering practice are turbulent in nature." [24]

2.3.7 Compressible and Incompressible Flows

2.3.7.1 Compressible Flow

"It is that type of flow in which the density ρ of the fluid changes from point to point (or in other words density is not constant for this flow).

Mathematically,

$$\rho \neq \text{constant}.$$

Example: Flow of gases through orifices, nozzles, gas turbines, etc." [24]

2.3.7.2 Incompressible Flow

"It is that type of flow in which density is constant for the fluid flow. Liquids are generally considered flowing incompressibly. Mathematically,

$$\rho = \text{constant}.$$

Example: Subsonic aerodynamics." [24]

2.4 Porous Medium

A porous medium refers to a material containing voids or pores that allow fluid (such as liquids or gases) to pass through. These voids can vary in size and shape, and the material itself can range from natural substances like soil and rock to engineered materials such as ceramics and foams.
Key characteristics of porous media include:

2.4.1 Permeability

This describes how easily fluids can flow through the material. It depends on factors like pore size, shape, and connectivity.

2.4.2 Porosity

This is the fraction of the total volume of the material that is occupied by voids or pores. It indicates the potential storage capacity for fluids within the medium.

Porous media are important in various fields such as geology, hydrology, civil engineering, chemical engineering, and biology.

They play a crucial role in processes like groundwater flow, oil extraction, filtration, and catalysis. The behavior of fluids in porous media is often complex and can

be described by various mathematical models, including Darcy's law for fluid flow and models for solute transport.

2.5 Darcy Forchheimer Porous Flow

A fluid flow regime through porous media in which Forchheimer's quadratic resistance law and Darcy's law are both simultaneously applicable is known as a Darcy-Forchheimer flow. An explanation of each part is provided below:

2.5.1 Darcy's Law

This principle asserts that the flow velocity (μ) is directly proportional to the pressure gradient and characterizes the movement of fluid through a porous medium, such as soil or a filter.

$$v = -\frac{k}{\mu}\nabla p,$$

where, v is the velocity vector, k is the permeability of the porous medium, μ is the dynamic viscosity of the fluid and ∇p is the pressure gradient.

2.5.2 Forchheimer's Law

This law extends Darcy's law by incorporating a quadratic resistance term to account for inertial effects at higher flow velocities:

$$v = -\frac{k}{\mu}\nabla p - \frac{B}{\mu}v|v|,$$

where, B is the Forchheimer coefficient, $\mathbf{v}|\mathbf{v}|$ represents the magnitude of the velocity vector squared.

When both Forchheimer's law and Darcy's law hold true, it means that viscous forces (which are governed by Darcy's law) and inertial forces (which are accounted

for by Forchheimer's law) combine to characterize the flow through the porous medium.

Applications of Darcy-Forchheimer flow can be found in many natural and engineering systems, including groundwater flow, oil reservoir engineering, filtration processes, and more, where fluid flow through porous media needs to be accurately modeled.

2.6 Darcy Forchheimer Medium

This is known as the Darcy-Forchheimer equation, which represents fluid flow through porous media. It extends the application of Darcy's law to laminar flow by including additional terms to account for inertial and non-linear effects that become significant at higher flow velocities or in more complex porous structures. The equation typically appears like this:

$$\Delta P = -\frac{\mu}{k}Q - \frac{\rho}{k}\alpha Q^2,$$

where, ΔP is the pressure drop across the porous medium, μ is the dynamic viscosity of the fluid, k is the permeability of the porous medium, ρ is the fluid density, α is the Forchheimer coefficient and Q is the volumetric flow rate.
The Darcy term in this equation is represented by the first term on the right-hand side.

It is inversely proportional to the permeability k and proportional to the flow rate Q. The Forchheimer effect is taken into account by the second term, which is proportional to Q^2.

This effect becomes significant in more complex geometries or at higher flow rates. When flow through porous media changes from laminar to turbulent or when the porosity and geometry of the medium have a substantial impact on the flow characteristics, the Darcy-Forchheimer equation comes in handy.

2.7 Heat and Mass Transfer Phenomenon and Related Properties

Heat transfer is the phenomenon of transferring energy and entropy from one place to another. The formal definition of heat transfer and its different types are given below.

2.7.1 Heat Transfer

"Heat transfer is a branch of engineering that deals with the transfer of thermal energy from one point to another within a medium or from one medium to another due to the occurrence of a temperature difference. Heat transfer may take place in one or more of its three basic forms: conduction, convection, and radiation." [25]

2.7.2 Mass Transfer

"Mass transfer is the flow of molecules from one body to another when these bodies are in contact or within a system consisting of two components when the distribution of materials is not uniform. When a copper plate is placed on a steel plate, some molecules from either side will diffuse into the other side.

When salt is placed in a glass and water poured over it, after sufficient time the salt molecules will diffuse into the water body. A more common example is drying of clothes or the evaporation of water spilled on the floor when water molecules diffuse into the air surrounding it.

Usually, mass transfer takes place from a location where the particular component is proportionately high to a location where the component is proportionately low. Mass transfer may also take place due to potentials other than concentration difference." [27]

2.7.3 Conduction

"Conduction is the transfer of heat from one part of a body at a higher temperature to another part of the same body at a lower temperature, or from one body at a higher temperature to another body in physical contact with it at a lower temperature.

The conduction process takes place at the molecular level and involves the transfer of energy from the more energetic molecules to those with a lower energy level. This can be easily visualized within gases, where we note that the average kinetic energy of molecules in the higher-temperature regions is greater than that of those in the lower-temperature regions.

The more energetic molecules, being in constant and random motion, periodically collide with molecules of a lower energy level and exchange energy and momentum. In this manner, there is a continuous transport of energy from the high-temperature regions to those of lower temperature. In liquids, the molecules are more closely spaced than in gases, but the molecular energy exchange process is qualitatively similar to that in gases. In the solids that are nonconductors of electricity (dielectrics), heat is conducted by lattice waves caused by atomic motion. In the solids that are good conductors of electricity, this lattice vibration mechanism is only a small contribution to the energy transfer process, the principal contribution being that due to the motion of free electrons, which move in a similar way to molecules in a gas." [28]

2.7.4 Convection

"The process of heat transfer between a surface and a fluid flowing in contact with it is called convection." [27]

2.7.4.1 Types of Convection

Natural Convection or Free Convection

"If the flow is caused by the buoyant forces generated by heating or cooling of the fluid the process is called as natural or free convection." [27]

Forced Convection

"If the flow is caused by an external device like a pump or blower, it is termed as forced convection." [27]

2.7.5 Radiation

"Radiation, or more correctly thermal radiation, is electromagnetic radiation emitted by a body by virtue of its temperature and at the expense of its internal energy. Thus thermal radiation is of the same nature as visible light, X-rays, and radio waves, the difference between them being in their wavelengths and the source of generation.

The eye is sensitive to electromagnetic radiation in the region from 0.39 to 0.78 μm; this is identified as the visible region of the spectrum. Radio waves have a wavelength of 1×10^3 to 2×10^{10} μm, and X-rays have wavelengths of 1×10^{-5} to 2×10^{-2} μm, while the bulk of thermal radiation occurs in rays from approximately 0.1 to 100 μm.

All heated solids and liquids, as well as some gases, emit thermal radiation. The transfer of energy by conduction requires the presence of a material medium, while radiation does not.

In fact, radiation transfer occurs most efficiently in a vacuum. On the macroscopic level, the calculation of thermal radiation is based on the Stefan-Boltzmann law, which relates the energy flux emitted by an ideal radiator (or blackbody) to the fourth power of the absolute temperature." [28]

2.7.6 Newtonian Fluid

"Fluids for which the applied shear stress and the rate of deformation are linearly proportional to each other are termed as Newtonian fluids.

In the case of Newtonian fluids, mathematical expression of τ_{xy} is given by expression enumerated underneath.

$$\tau_{xy} = \mu \frac{du}{dy},$$

where, μ represents dynamic viscosity and $\frac{du}{dy}$ is the rate of deformation. The SI unit of shear stress τ_{xy} is N·s.m^2." [29]

2.7.7 Non-Newtonian Fluid

"A non-Newtonian fluid is one whose properties are different from Newtonian fluids i.e. apparent viscosity changes with applied stress or forces. In non-Newtonian fluid the correlation between the shear stress and the rate of strain is non-linear. For these types of fluids, the constant of proportionality, viscosity, may change with time. Many salt solution, solution of polymers as well as liquids in which fine particles are suspended, are non-Newtonian, as are most commonly found substances in our everyday life such as ketchup, toothpaste, paint, blood and shampoo." [30]

2.8 Fundamental Laws

2.8.1 Conservation of Mass, the Continuity Equation

"The principle of conservation of mass can be stated as the time rate of change of mass in a fixed volume is equal to the net rate of flow of mass across the surface.

The mathematical statement of the principle results in the following equation, known as the continuity (of mass) equation

$$\frac{\partial \rho}{\partial t} + \nabla.(\rho \mathbf{v}) = 0 \tag{2.1}$$

where ρ is the density of the medium, $\mathbf{v}$ the velocity vector, and ∇ is the nabla or del operator. The continuity equation in (2.1) is in conservation (or divergence) form since it can be derived directly from an integral statement of mass conservation. By introducing the material derivative or Eulerian derivative operator $\frac{D}{Dt}$

$$\frac{D}{Dt} = \frac{\partial}{\partial t} + \mathbf{v}.\nabla, \tag{2.2}$$

the continuity equation (2.1) can be expressed in the alternate, non-conservation (or advective) form

$$\frac{\partial \rho}{\partial t} + \mathbf{v}.\nabla\rho + \rho\nabla.\mathbf{v} = \frac{D\rho}{Dt} + \rho\nabla.\mathbf{v} = 0 \tag{2.3}$$

For steady-state conditions, the continuity equation becomes

$$\nabla.(\rho \mathbf{v}) = 0 \tag{2.4}$$

When the density changes following a fluid particle are negligible, the continuum is termed incompressible and we have $\frac{D\rho}{Dt} = 0$. The continuity equation (2.3) then becomes

$$\nabla.\mathbf{v} = 0 \tag{2.5}$$

which is often referred to as the incompressibility condition or incompressibility constraint." [25]

2.8.2 Conservation of Momentum

"The principle of conservation of linear momentum (or Newton's Second Law of motion) states that the time rate of change of linear momentum of a given set

of particles is equal to the vector sum of all the external forces acting on the particles of the set, provided Newton's Third Law of action and reaction governs the internal forces. Newton's Second Law can be written as

$$\frac{\partial \rho \mathbf{v}}{\partial t} + \nabla.(\rho \mathbf{v} \otimes \mathbf{v}) = \nabla.\sigma + \rho \mathbf{f} \tag{2.6}$$

where $\otimes$ is the tensor (or dyadic) product of two vectors, σ is the Cauchy stress tensor (N/m^2) and $\mathbf{f}$ is the body force vector, measured per unit mass and normally taken to be the gravity vector.

Equation (2.6) describes the motion of a continuous medium, and in fluid mechanics they are also known as the Navier equations. The form of the momentum equation shown in (2.6) is the conservation (divergence) form that is most often utilized for compressible flows.

This equation may be simplified to a form more commonly used with incompressible flows. Expanding the first two derivatives and collecting terms

$$\rho\left(\frac{\partial \mathbf{v}}{\partial t} + \mathbf{v}\nabla.\mathbf{v}\right) + \mathbf{v}\left(\frac{\partial \rho}{\partial t} + \nabla.\rho\mathbf{v}\right) = \nabla.\sigma + \rho\mathbf{f} \tag{2.7}$$

The second term in parentheses is the continuity equation (2.1) and neglecting this term allows (2.7) to reduce to the non-conservation (advective) form

$$\rho\frac{D\mathbf{v}}{Dt} = \nabla.\sigma + \rho\mathbf{f} \tag{2.8}$$

where the material derivative (2.2) has been employed.

The principle of conservation of angular momentum can be stated as the time rate of change of the total moment of momentum of a given set of particles is equal to the vector sum of the moments of the external forces acting on the system.
In the absence of distributed couples, the principle leads to the symmetry of the stress tensor:

$$\sigma = (\sigma)^T \tag{2.9}$$

where the superscript T denotes the transpose of the enclosed quantity." [25]

2.8.3 Conservation of Energy

"The law of conservation of energy (or the First Law of Thermodynamics) states that the time rate of change of the total energy is equal to the sum of the rate of work done by applied forces and the change of heat content per unit time. In the general case, the First Law of Thermodynamics can be expressed in conservation form as

$$\frac{\partial \rho e^t}{\partial t} + \nabla.\rho \mathbf{v} e^t = -\nabla.\mathbf{q} + \nabla.(\sigma.\mathbf{v}) + Q + \rho \mathbf{f}.\mathbf{v} \tag{2.10}$$

where $e^t = e + 1/2\mathbf{v}.\mathbf{v}$ is the total energy (J/m^3), e is the internal energy, $\mathbf{q}$ is the heat flux vector (W/m^2) and Q is the internal heat generation (W/m^3). The total energy equation (2.10) is useful for high speed compressible flows where the kinetic energy is significant. For incompressible flows, an internal energy equation is more appropriate and can be derived from (2.10) with use of the momentum equation (2.6). Taking the dot product of the velocity vector with the momentum equation produces an equation for the kinetic energy; this equation is subtracted from the total energy equation (2.10) to produce the conservation (divergence) form of the internal energy equation

$$\frac{\partial \rho e}{\partial t} + \nabla.\rho \mathbf{v} e = -\nabla.\mathbf{q} + Q + \Phi \tag{2.11}$$

where Φ is a dissipation function that is defined by

$$\Phi = \sigma : \nabla \mathbf{v} \tag{2.12}$$

In (2.12) $\nabla \mathbf{v}$ is the velocity gradient tensor which will be defined more completely in the following sections. The thermal energy equation in (2.11) can be simplified further by expanding the derivatives on the left-hand side of the equation and using the continuity equation. The resulting equation is the non-conservative

(advective) form of the energy equation

$$\rho \frac{De}{Dt} = -\nabla.\mathbf{q} + Q + \Phi \tag{2.13}$$

which is the standard form used for incompressible flows. Constitutive relations for e and $\mathbf{q}$ will be defined in the next sections and allow (2.13) to be expressed in terms of the temperature T."

Chapter 3

Fundamentals of the Finite Element Method

The Finite Element Method (FEM) shares numerous conceptual foundations with the Finite Volume Method (FVM). In two-dimensional analysis, the computational domain is discretized into simple geometrical elements such as triangles or quadrilaterals, whereas in three-dimensional applications, tetrahedra or hexahedra are predominantly used.

Prior to integration over the domain, the governing equations are multiplied by weight functions. In basic FEM applications, continuity across adjacent elements is ensured by approximating the solution within each element using linear shape functions derived from nodal values.

By substituting the approximate solution into the weighted integral form of the governing conservation laws and demanding that the derivative of the integral with respect to each nodal value vanish, a discrete system of equations is derived. To illustrate the FEM procedure, a simple two-dimensional Poisson equation is solved as a representative case study, in this chapter

3.1 Finite Element Approaches

The development of FEM models can follow several methodological frameworks: For instance,

(i) Direct Method

(ii) Variational Method

(iii) Method of Weighted Residuals

Among these, the method of weighted residuals is especially suitable for problems expressed in the form of differential equations. Below we briefly describe the method of weighted residual.

3.1.1 Method of Weighted Residual

Consider a boundary value problem represented by the differential equation

$$\mathcal{L}u = f(x), \tag{3.1}$$

where $f(x)$ is a known source function, $u(x)$ is the unknown solution, and $\mathcal{L}$ is a differential operator. An approximate solution $\tilde{u}(x)$ is introduced that satisfies the prescribed boundary conditions but not necessarily the governing equation, resulting in a residual

$$R(\tilde{u}) = \mathcal{L}\tilde{u} - f \neq 0. \tag{3.2}$$

Assume a trial solution of the form

$$\tilde{u}(x) = \sum_{i=1}^{N} u_i \phi_i(x), \tag{3.3}$$

where, $\phi_i(x)$ are the basis functions. Since the space spanned by ϕ_i is finite-dimensional, the residual $R(\tilde{u})$ is generally non-zero within the domain.

To minimize the residual in (3.2), we enforce the condition

$$\int_{\Omega} w(x)R(\tilde{u})\,d\Omega = 0, \tag{3.4}$$

for a set of weight functions $w(x)$ constructed as:

$$w(x) = \sum_{i=1}^{N} w_i \psi_i(x), \tag{3.5}$$

where $\psi_i(x)$ are known functions and w_i are scalar coefficients to determine.

This leads to a system of equations of the form:

$$[A]\mathbf{u} = \mathbf{F}, \tag{3.6}$$

where $[A]$ is the system stiffness matrix and $\mathbf{u}$ contains the unknown coefficients, and F is the system source vector.

Example 1:

In this example, we consider a one-dimensional boundary value problem to demonstrate the working methodology of weighted residual method.

Consider, solving the differential equation:

$$\frac{d^2u}{dx^2} - u = -x, \quad \text{for } 0 < x < 1, \quad u(0) = u(1) = 0. \tag{3.7}$$

Choose a trial function that satisfies the boundary conditions

$$\tilde{u}(x) = ax(1-x). \tag{3.8}$$

Substitute (3.8) into the differential equation in (3.7) to compute the residual. This simplifies

$$R(x) = \frac{d^2\tilde{u}}{dx^2} - \tilde{u} + x = -2a - ax(1-x) + x. \tag{3.9}$$

Expanding and simplifying (3.9) gives

$$R(x) = -2a - ax + ax^2 + x. \tag{3.10}$$

Using the Galerkin method, the weight function is chosen as

$$w(x) = \frac{d\tilde{u}}{da} = x(1-x). \tag{3.11}$$

The weighted residual condition in (3.10) becomes

$$\int_0^1 (x - x^2)(-2a - ax + ax^2 + x)\, dx = 0. \tag{3.12}$$

Solving the above integral yields $a \approx 0.2267$. From (3.8), we can write

$$\tilde{u}(x) = 0.2267x(1-x). \tag{3.13}$$

This is the solution of the considered boundary value problem in (3.7).

3.2 Galerkin Finite Element Method

The GFEM procedural steps are given as below

Step 1: Discretize the domain $\Omega = [c, d]$, $c, d \in \mathbb{R}$, into L number of elements using nodal points $y_0 = c, y_1, ..., y_L = d$. Define element size $h_i = y_{i+1} - y_i$. Convert the strong form of the governing equation into a weak form by multiplying with test functions and applying integration by parts.

Step 3: Choose an approximate test space V_h for trial and test functions. Usually we choose space of Polynomials. Apply Galerkin discretization: Find $v_h \in V_h$ such that

$$a(v_h, w_h) = b(w_h), \quad \forall w_h \in W_h.$$

Step 5: Represent the approximate solution as follows

$$v_h^e = \sum_{j=1}^{NEN} v_j^e \varphi_j^e, \qquad w_h^e = \sum_{i=1}^{NEN} w_i^e \varphi_i^e. \tag{3.14}$$

Step 6: Substituting into the weak formulation leads to

$$\sum_{j=1}^{NEN} a(\varphi_j^e, \varphi_i^e) v_j^e = b(\varphi_i^e). \tag{3.15}$$

Step 7: Obtain the matrix form,

$$[A^e]\{v^e\} = \{B^e\}. \tag{3.16}$$

Step 8: Assemble all elemental matrices into a global system

$$[A]\{v\} = \{B\}. \tag{3.17}$$

Step 9: Solve the system in (3.17) using different numerical methods, i-e Conjugate Gradient Method.

Example 2: (Two-Dimensional Poisson equation)

Consider the steady two-dimensional Poisson equation as follows.

$$-\nabla \cdot (\nabla S) = f \quad \text{in } \Omega, \tag{3.18}$$

$$S = 0 \quad \text{on } \partial\Omega. \tag{3.19}$$

To solve (3.17) and(3.18) we define $H_0^1(\Omega)$, a Sobolev space is a vector space of functions equipped with a norm that is a combination of L^p -norms of the function together with its derivatives up to a given order.

Multiplying (3.18) by a test function $w(x, y) \in H_0^1(\Omega)$ and integrating over Ω, we get

$$\int_{\Omega^e} \left(\frac{\partial w}{\partial x}\frac{\partial S}{\partial x} + \frac{\partial w}{\partial y}\frac{\partial S}{\partial y} \right) d\Omega = \int_{\Omega^e} w f \, d\Omega. \tag{3.20}$$

Approximate the solution over element e by

$$S^e(x,y) = \sum_{j=1}^{NEN} S_j^e \varphi_j^e(x,y), \tag{3.21}$$

where NEN represents the total number of finite elements in the discretized domain. Substitute (3.21) into the weak form in (3.20) implies

$$\sum_{j=1}^{NEN} \left[\int_{\Omega^e} \left(\frac{\partial \varphi_j^e}{\partial x} \frac{\partial \varphi_i^e}{\partial x} + \frac{\partial \varphi_j^e}{\partial y} \frac{\partial \varphi_i^e}{\partial y} \right) d\Omega \right] S_j^e = \int_{\Omega^e} \varphi_i^e f \, d\Omega. \tag{3.22}$$

This yields the elemental system equation as below.

$$A^e S^e = F^e. \tag{3.23}$$

Now, assembling all elemental equation leads to the global system

$$AS = F. \tag{3.24}$$

Solving the above system yields the approximate solution over the domain Ω.

Chapter 4

Mathematical Modeling of Radiative Transport in Porous Media

This chapter presents a mathematical model and comprehensive analysis of radiation effects in fluid flow through a porous medium. The study begins by transforming the governing partial differential equations (PDEs) from their dimensional form into a dimensionless form, thereby simplifying the mathematical model for numerical computation. These equations are then reformulated into their weak form, which is essential for implementation using the Galerkin Finite Element Method.

4.1 Geometry of the Problem

The figure 4.1 illustrates the geometry of a lid-driven square cavity, a classic benchmark problem in computational fluid dynamics. The cavity consists of a square enclosure with distinct boundary conditions on each wall. The bottom wall is maintained at a constant high temperature ($T = 1$), representing the hot surface, while the top wall acts as a cold moving lid ($T = 0$), which simultaneously imposes

a shear-driven flow and introduces thermal gradients. The vertical sidewalls are adiabatic, meaning no heat transfer occurs through them. The lid-driven motion at the top induces fluid circulation inside the cavity, which interacts with the thermal boundary conditions to create a complex coupling between momentum and heat transfer. This configuration is widely used to study convection, fluid mixing, and the influence of thermal and flow parameters in enclosed domains.

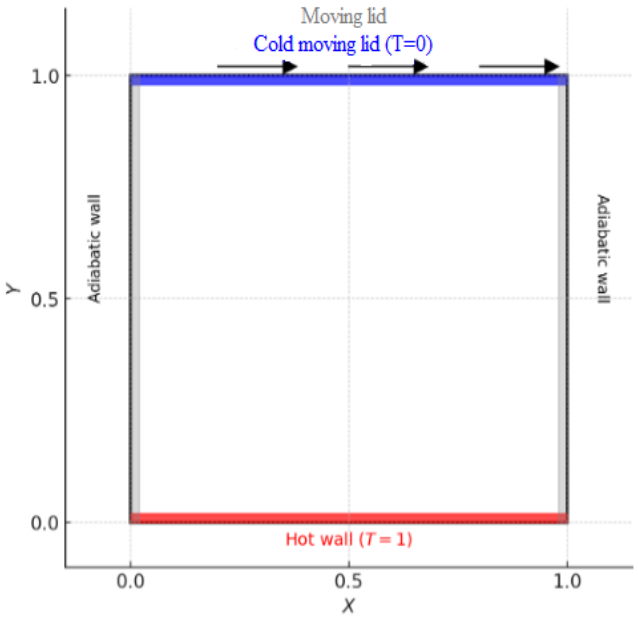

FIGURE 4.1: Geometry of the lid-driven square cavity.

4.2 Governing Equations in Vector-Tensor Form

The mathematical modeling of flow and heat transfer in the presence of radiation is governed by a system of coupled partial differential equations. These include the continuity equation, momentum conservation equation, and energy equation—expressed in vector-tensor form to capture the multidimensional nature of the physical phenomena.

The governing equations are as follows. The continuity equation

$$\nabla \cdot \boldsymbol{u} = 0, \tag{4.1}$$

ensure mass conservation for incompressible flow under consideration. The equation

$$\rho\left(\frac{\partial \boldsymbol{u}}{\partial \tilde{t}} + (\boldsymbol{u}\cdot\nabla)\,\boldsymbol{u}\right) - \mu\nabla^2\boldsymbol{u} + \nabla p + P_v\boldsymbol{u} + P_i|\boldsymbol{u}|^2 = 0, \tag{4.2}$$

is the momentum equation, accounting for viscous effects, inertial forces, pressure gradients, and flow resistance within the porous medium.

The last two terms of (4.2) are the flow resistance terms. The term $P_v\boldsymbol{u}$ is the Darcy term and the term $P_i|\boldsymbol{u}|^2$ is the Forchheimer term.

The equation

$$\rho C_p\left(\frac{\partial \tilde{T}}{\partial \tilde{t}} + (\boldsymbol{u}\cdot\nabla)\,\tilde{T}\right) - k\nabla^2\tilde{T} + \frac{\partial q_r}{\partial y} = 0, \tag{4.3}$$

is the energy equation, which governs heat transport through convection, conduction, and radiative flux q_r in the direction vertical to flow.

These equations provide the foundational framework for numerical simulation and are critical for accurately capturing the interaction between fluid dynamics and thermal radiation in porous media.

4.3 Conversion to Component Form

To facilitate numerical implementation and gain deeper insight into the behavior of individual velocity and temperature components, the vector-tensor form of the governing equations is converted into their corresponding component form. This transformation expresses each physical quantity in Cartesian coordinates, making the equations more tractable for finite element discretization.

The component form of the governing equations is presented below.

The incompressibility condition is given by the general vector form:

$$\nabla \cdot \boldsymbol{u} = 0.$$

By expanding in Cartesian coordinates, we get

$$\left(\frac{\partial}{\partial x}, \frac{\partial}{\partial y}\right) \cdot (u, v) = \frac{\partial u}{\partial x} + \frac{\partial v}{\partial y},$$

which simplifies to the scalar form:

$$\frac{\partial u}{\partial x} + \frac{\partial v}{\partial y} = 0. \tag{4.4}$$

The momentum equation in its general vector form is related as

$$\rho\left(\frac{\partial \boldsymbol{u}}{\partial \tilde{t}} + (\boldsymbol{u} \cdot \nabla)\,\boldsymbol{u}\right) - \mu\nabla^2\boldsymbol{u} + \nabla p + P_v\boldsymbol{u} + P_i|\boldsymbol{u}|^2 = 0.$$

Expanding the nonlinear convective term:

$$\begin{aligned}(\mathbf{u} \cdot \nabla)\mathbf{u} &= (u, v) \cdot \left(\frac{\partial}{\partial x}, \frac{\partial}{\partial y}\right)(u, v) \\ &= \left(u\frac{\partial}{\partial x} + v\frac{\partial}{\partial y}\right)(u, v) \\ &= \Big(u\,\partial_x u + v\,\partial_y u,\ u\,\partial_x v + v\,\partial_y v\Big).\end{aligned}$$

Expanding the viscous diffusion term:

$$\nabla^2\boldsymbol{u} = \left(\frac{\partial^2 u}{\partial x^2} + \frac{\partial^2 u}{\partial y^2},\ \frac{\partial^2 v}{\partial x^2} + \frac{\partial^2 v}{\partial y^2}\right).$$

Now, rewriting the x-component of the momentum equation:

$$\rho\left(\frac{\partial u}{\partial \tilde{t}} + u\frac{\partial u}{\partial x} + v\frac{\partial u}{\partial y}\right) - \mu\left(\frac{\partial^2 u}{\partial x^2} + \frac{\partial^2 u}{\partial y^2}\right) + \frac{\partial p}{\partial x} + P_v u + P_i(u^2 + v^2) = 0,$$

$$\Rightarrow \frac{\partial u}{\partial \tilde{t}} + u\frac{\partial u}{\partial x} + v\frac{\partial u}{\partial y} = -\frac{1}{\rho}\frac{\partial p}{\partial x} + \frac{\mu}{\rho}\left(\frac{\partial^2 u}{\partial x^2} + \frac{\partial^2 u}{\partial y^2}\right) - \frac{P_v}{\rho}u - \frac{P_i}{\rho}(u^2 + v^2). \quad (4.5)$$

Momentum equation in the y-direction is expressed as

$$\rho\left(\frac{\partial v}{\partial \tilde{t}} + u\frac{\partial v}{\partial x} + v\frac{\partial v}{\partial y}\right) - \mu\left(\frac{\partial^2 v}{\partial x^2} + \frac{\partial^2 v}{\partial y^2}\right) + \frac{\partial p}{\partial y} + P_v v + P_i(u^2 + v^2) = 0.$$

Energy Equation in vector form reads:

$$\rho C_p\left(\frac{\partial \tilde{T}}{\partial \tilde{t}} + (\boldsymbol{u}\cdot\nabla)\,\tilde{T}\right) - k\nabla^2\tilde{T} + \frac{\partial q_r}{\partial y} = 0.$$

Energy equation, when expanded in scalar form reads:

$$\rho C_p\left(\frac{\partial \tilde{T}}{\partial \tilde{t}} + u\frac{\partial \tilde{T}}{\partial x} + v\frac{\partial \tilde{T}}{\partial y}\right) - k\left(\frac{\partial^2 \tilde{T}}{\partial x^2} + \frac{\partial^2 \tilde{T}}{\partial y^2}\right) + \frac{\partial q_r}{\partial y} = 0.$$

Energy equation after simplification reads:

$$\frac{\partial \tilde{T}}{\partial \tilde{t}} + u\frac{\partial \tilde{T}}{\partial x} + v\frac{\partial \tilde{T}}{\partial y} = \frac{k}{\rho C_p}\left(\frac{\partial^2 \tilde{T}}{\partial x^2} + \frac{\partial^2 \tilde{T}}{\partial y^2}\right) - \frac{1}{\rho C_p}\frac{\partial q_r}{\partial y}. \quad (4.6)$$

The terms P_v and P_i in (4.5), represents porous medium resistance coefficients (Darcy and Forchheimer), and q_r is the radiative heat flux in the y-direction.

The governing equations for unsteady, incompressible, and viscous fluid motion with radiative heat transfer through a porous medium can be formulated in Cartesian coordinates (x, y). These consist of the continuity equation, the momentum equations along the x- and y-directions, together with the energy equation.

Continuity equation:

$$\frac{\partial u}{\partial x} + \frac{\partial v}{\partial y} = 0. \quad (4.7)$$

Momentum equation in x-direction:

$$\frac{\partial u}{\partial \tilde{t}} + u\frac{\partial u}{\partial x} + v\frac{\partial u}{\partial y} = -\frac{1}{\rho}\frac{\partial p}{\partial x} + \frac{\mu}{\rho}\left(\frac{\partial^2 u}{\partial x^2} + \frac{\partial^2 u}{\partial y^2}\right) - \frac{P_v}{\rho}u - \frac{P_i}{\rho}(u^2 + v^2). \tag{4.8}$$

Momentum equation in y-direction:

$$\frac{\partial v}{\partial \tilde{t}} + u\frac{\partial v}{\partial x} + v\frac{\partial v}{\partial y} = -\frac{1}{\rho}\frac{\partial p}{\partial y} + \frac{\mu}{\rho}\left(\frac{\partial^2 v}{\partial x^2} + \frac{\partial^2 v}{\partial y^2}\right) - \frac{P_v}{\rho}v - \frac{P_i}{\rho}(u^2 + v^2). \tag{4.9}$$

Energy equation:

$$\frac{\partial \tilde{T}}{\partial \tilde{t}} + u\frac{\partial \tilde{T}}{\partial x} + v\frac{\partial \tilde{T}}{\partial y} = \frac{k}{\rho C_p}\left(\frac{\partial^2 \tilde{T}}{\partial x^2} + \frac{\partial^2 \tilde{T}}{\partial y^2}\right) - \frac{1}{\rho C_p}\frac{\partial q_r}{\partial y}. \tag{4.10}$$

The Dimensional Boundary Conditions

$$u = u_o, \quad v = 0 \quad \forall \quad x \in [0,1] \quad \text{and} \quad y = 1.$$

$$u = v = 0 \quad \forall \quad x \in [0,1], \quad \text{and} \quad y = 0.$$

$$u = v = 0 \quad \forall \quad x \in \{0,1\} \quad \text{and} \quad y \in [0,1].$$

$$\tilde{T} = 1 + T_\infty \quad \forall \quad x \in [0,1] \quad \text{and} \quad y = 0.$$

$$\tilde{T} = 0 \quad \forall \quad x \in [0,1] \quad \text{and} \quad y = 1.$$

$$\frac{\partial \tilde{T}}{\partial x} \quad \forall \quad x \in \{0,1\} \quad \text{and} \quad y \in [0,1].$$

$$\frac{\partial \tilde{T}}{\partial x} \quad \forall \quad x = 1 \quad \text{and} \quad y \in [0,1].$$

$$\frac{\partial \tilde{T}}{\partial x} \quad \forall \quad x = 0 \quad \text{and} \quad y \in [0,1].$$

In these equations, u and v denote the velocity components along the x- and y-axes, respectively. The variable p refers to the pressure, while $\tilde{T}$ indicates the temperature field. The term q_r corresponds to the radiative heat flux in the y-direction. Furthermore, P_v and P_i denote the resistance parameters of the porous medium, associated with Darcy and Forchheimer contributions, respectively.

Consider,

$$U = \frac{u}{u_o}, \quad V = \frac{v}{u_o}, \quad t = \frac{u_o}{L}\tilde{t}, \quad X = \frac{x}{L}, \quad Y = \frac{y}{L}, \quad P = \frac{p}{\rho u_o^2} \quad \text{and} \quad T = \tilde{T} + T_\infty, \tag{4.11}$$

as the dimensionless parameters.

4.4 Conversion of Dimensional Equations into Dimensionless Equations

To convert equations (4.7)-(4.10) into the dimensionless form, certain derivatives are required which have been calculated here in this section.

$$X = \frac{x}{L} \quad \Rightarrow \quad \frac{\partial X}{\partial x} = \frac{1}{L}.$$

$$Y = \frac{y}{L} \quad \Rightarrow \quad \frac{\partial Y}{\partial y} = \frac{1}{L}.$$

$$U = \frac{u}{u_o} \quad \Rightarrow \quad u = u_o U.$$

$$V = \frac{v}{u_o} \quad \Rightarrow \quad v = u_o V.$$

$$\frac{\partial u}{\partial \tilde{t}} = \frac{\partial u}{\partial t}\frac{\partial t}{\partial \tilde{t}} = \frac{\partial}{\partial t}(u)\frac{\partial}{\partial \tilde{t}}t = \frac{\partial}{\partial t}(u_o U)\frac{\partial}{\partial \tilde{t}}\left(\frac{u_o}{L}\tilde{t}\right) = u_o\frac{\partial U}{\partial t}\frac{u_o}{L} = \frac{u_o^2}{L}\frac{\partial U}{\partial t}.$$

$$\frac{\partial u}{\partial x} = \frac{\partial u}{\partial X}\frac{\partial X}{\partial x} = \frac{\partial}{\partial X}(u)\frac{1}{L} = \frac{\partial}{\partial X}(u_o U)\frac{1}{L} = \frac{u_o}{L}\frac{\partial U}{\partial X}.$$

$$\frac{\partial u}{\partial y} = \frac{\partial u}{\partial Y}\frac{\partial Y}{\partial y} = \frac{\partial}{\partial Y}(u)\frac{1}{L} = \frac{\partial}{\partial Y}(u_o U)\frac{1}{L} = \frac{u_o}{L}\frac{\partial U}{\partial Y}.$$

$$\frac{\partial v}{\partial y} = \frac{\partial v}{\partial Y}\frac{\partial Y}{\partial y} = \frac{\partial}{\partial Y}(v)\frac{1}{L} = \frac{\partial}{\partial Y}(u_o V)\frac{1}{L} = \frac{u_o}{L}\frac{\partial V}{\partial Y}.$$

$$u\frac{\partial u}{\partial x} = u_o U\frac{u_o}{L}\frac{\partial U}{\partial X} = \frac{u_o^2}{L}U\frac{\partial U}{\partial X}.$$

$$v\frac{\partial u}{\partial y} = u_o V\frac{u_o}{L}\frac{\partial U}{\partial Y} = \frac{u_o^2}{L}V\frac{\partial U}{\partial Y}.$$

$$\frac{\partial^2 u}{\partial x^2} = \frac{\partial}{\partial x}\left(\frac{\partial u}{\partial x}\right) = \frac{\partial}{\partial x}\left(\frac{u_o}{L}\frac{\partial U}{\partial X}\right) = \frac{\partial}{\partial X}\frac{\partial X}{\partial x}\left(\frac{u_o}{L}\frac{\partial U}{\partial X}\right) = \frac{\partial}{\partial X}\frac{1}{L}\left(\frac{u_o}{L}\frac{\partial U}{\partial X}\right).$$

$$\frac{\partial^2 u}{\partial x^2} = \frac{u_o}{L^2}\frac{\partial^2 U}{\partial X^2}.$$

$$\frac{\partial^2 u}{\partial y^2} = \frac{\partial}{\partial y}\left(\frac{\partial u}{\partial y}\right) = \frac{\partial}{\partial y}\left(\frac{u_o}{L}\frac{\partial U}{\partial Y}\right) = \frac{\partial}{\partial Y}\frac{\partial Y}{\partial y}\left(\frac{u_o}{L}\frac{\partial U}{\partial Y}\right) = \frac{\partial}{\partial Y}\frac{1}{L}\left(\frac{u_o}{L}\frac{\partial U}{\partial Y}\right).$$

$$\frac{\partial^2 u}{\partial y^2} = \frac{u_o}{L^2}\frac{\partial^2 U}{\partial Y^2}.$$

$$\frac{\partial v}{\partial \tilde{t}} = \frac{\partial v}{\partial t}\frac{\partial t}{\partial \tilde{t}} = \frac{\partial}{\partial t}(v)\frac{\partial}{\partial \tilde{t}}t = \frac{\partial}{\partial t}(u_o V)\frac{\partial}{\partial \tilde{t}}\left(\frac{u_o}{L}\tilde{t}\right) = u_o\frac{\partial V}{\partial t}\frac{u_o}{L} = \frac{u_o^2}{L}\frac{\partial V}{\partial t}.$$

$$\frac{\partial v}{\partial x} = \frac{\partial v}{\partial X}\frac{\partial X}{\partial x} = \frac{\partial}{\partial X}(v)\frac{1}{L} = \frac{\partial}{\partial X}(u_o V)\frac{1}{L} = \frac{u_o}{L}\frac{\partial V}{\partial X} = u_o U\frac{u_o}{L}\frac{\partial V}{\partial X} = \frac{u_o^2}{L}U\frac{\partial V}{\partial X}.$$

$$v\frac{\partial v}{\partial y} = u_o V\frac{u_o}{L}\frac{\partial V}{\partial Y} = \frac{u_o^2}{L}V\frac{\partial V}{\partial Y}.$$

$$\frac{\partial^2 v}{\partial x^2} = \frac{\partial}{\partial x}\left(\frac{\partial u}{\partial x}\right) = \frac{\partial}{\partial x}\left(\frac{u_o}{L}\frac{\partial V}{\partial X}\right) = \frac{\partial}{\partial X}\frac{\partial X}{\partial x}\left(\frac{u_o}{L}\frac{\partial V}{\partial X}\right) = \frac{\partial}{\partial X}\frac{1}{L}\left(\frac{u_o}{L}\frac{\partial V}{\partial X}\right).$$

$$\frac{\partial^2 v}{\partial x^2} = \frac{u_o}{L^2}\frac{\partial^2 V}{\partial X^2}.$$

$$\frac{\partial^2 v}{\partial y^2} = \frac{\partial}{\partial y}\left(\frac{\partial v}{\partial y}\right) = \frac{\partial}{\partial y}\left(\frac{u_o}{L}\frac{\partial V}{\partial Y}\right) = \frac{\partial}{\partial Y}\frac{\partial Y}{\partial y}\left(\frac{u_o}{L}\frac{\partial V}{\partial Y}\right) = \frac{\partial}{\partial Y}\frac{1}{L}\left(\frac{u_o}{L}\frac{\partial V}{\partial Y}\right).$$

$$\frac{\partial^2 v}{\partial y^2} = \frac{u_o}{L^2}\frac{\partial^2 V}{\partial Y^2}.$$

$$\frac{\partial \tilde{T}}{\partial \tilde{t}} = \frac{\partial \tilde{T}}{\partial t}\frac{\partial t}{\partial \tilde{t}} = \frac{\partial}{\partial t}(\tilde{T})\frac{\partial}{\partial \tilde{t}}t = \frac{\partial}{\partial t}(T+T_\infty)\frac{\partial}{\partial \tilde{t}}\left(\frac{u_o}{L}\tilde{t}\right) = \left(\frac{u_o}{L}\right)\frac{\partial T}{\partial t}.$$

$$\frac{\partial \tilde{T}}{\partial x} = \frac{\partial}{\partial X}\frac{\partial X}{\partial x}\tilde{T} = \frac{\partial}{\partial X}\frac{1}{L}(T+T_\infty) = \frac{1}{L}\frac{\partial T}{\partial X}.$$

$$\frac{\partial \tilde{T}}{\partial y} = \frac{\partial}{\partial Y}\frac{\partial Y}{\partial y}\tilde{T} = \frac{\partial}{\partial Y}\frac{1}{L}(T+T_\infty) = \frac{1}{L}\frac{\partial T}{\partial Y}.$$

$$u\frac{\partial \tilde{T}}{\partial x} = u_o U\frac{\partial}{\partial X}\frac{\partial X}{\partial x}\tilde{T} = u_o U\frac{\partial}{\partial X}\frac{1}{L}(T+T_\infty) = \frac{u_o}{L}U\frac{\partial T}{\partial X}.$$

$$v\frac{\partial \tilde{T}}{\partial y} = u_o V\frac{\partial}{\partial Y}\frac{\partial Y}{\partial y}\tilde{T} = u_o V\frac{\partial T}{\partial Y}\frac{1}{L}(T+T_\infty) = \frac{u_o}{L}V\frac{\partial T}{\partial Y}.$$

$$\frac{\partial^2 \tilde{T}}{\partial x^2} = \frac{\partial}{\partial x}\left(\frac{\partial \tilde{T}}{\partial x}\right) = \frac{\partial}{\partial x}\left(\frac{1}{L}\frac{\partial T}{\partial X}\right) = \frac{\partial}{\partial X}\frac{\partial X}{\partial x}\left(\frac{1}{L}\frac{\partial T}{\partial X}\right) = \frac{\partial}{\partial X}\frac{1}{L}\left(\frac{1}{L}\frac{\partial T}{\partial X}\right).$$

$$\frac{\partial^2 \tilde{T}}{\partial x^2} = \frac{1}{L^2}\frac{\partial^2 T}{\partial X^2}.$$

$$\frac{\partial^2 \tilde{T}}{\partial y^2} = \frac{\partial}{\partial y}\left(\frac{\partial \tilde{T}}{\partial y}\right) = \frac{\partial}{\partial Y}\frac{\partial Y}{\partial y}\left(\frac{1}{L}\frac{\partial T}{\partial Y}\right) = \frac{\partial}{\partial Y}\frac{1}{L}\left(\frac{1}{L}\frac{\partial T}{\partial Y}\right)\frac{\partial^2 \tilde{T}}{\partial y^2} = \frac{1}{L^2}\frac{\partial^2 T}{\partial Y^2}.$$

The radiative heat flux q_r can be expressed as:

$$q_r = -\frac{4\sigma}{3k}\frac{\partial T^4}{\partial y} = -\frac{16\sigma}{3k}T^3\frac{\partial T}{\partial y},$$

where, k is the absorption coefficient and σ is the Stefan–Boltzmann constant.

The Taylor series expansion of T^4 about the ambient temperature T_∞, assuming a relatively small temperature difference, is given by:

$$T^4 = T_\infty^4 + 4T_\infty^3(T - T_\infty) + 6T_\infty^2(T - T_\infty)^2 + \cdots .$$

Neglecting higher-order terms, we obtain the approximation:

$$T^4 \approx T_\infty^4 + 4T_\infty^3(T - T_\infty) = T_\infty^4 + 4T_\infty^3 T - 4T_\infty^4 = -3T_\infty^4 + 4T_\infty^3 T.$$

Substituting into the expression for q_r:

$$\begin{aligned} q_r &= -\frac{4\sigma}{3k}\frac{\partial T^4}{\partial y} \\ &= -\frac{4\sigma}{3k}\frac{\partial}{\partial y}(-3T_\infty^4 + 4T_\infty^3 T) \\ &= -\frac{4\sigma}{3k}\cdot 4T_\infty^3\frac{\partial T}{\partial y} \\ &= -\frac{16\sigma}{3k}T_\infty^3\frac{\partial T}{\partial y}. \end{aligned}$$

Define the dimensionless variables as:

$$x = LX, \quad y = LY, \quad u = u_0 U, \quad \text{and} \quad v = u_0 V$$

Taking partial derivatives:

$$\frac{\partial u}{\partial x} = \frac{u_0}{L}\frac{\partial U}{\partial X}, \quad \frac{\partial v}{\partial y} = \frac{u_0}{L}\frac{\partial V}{\partial Y}. \tag{4.12}$$

Substituting into the dimensional continuity equation:

$$\frac{\partial u}{\partial x} + \frac{\partial v}{\partial y} = 0. \tag{4.13}$$

Using (4.12) in (4.13), we get

$$\Rightarrow \frac{u_0}{L}\frac{\partial U}{\partial X} + \frac{u_0}{L}\frac{\partial V}{\partial Y} = 0.$$

after simplifying we get

$$\frac{u_0}{L}\left(\frac{\partial U}{\partial X} + \frac{\partial V}{\partial Y}\right) = 0.$$

Since $\frac{u_0}{L} \neq 0$, we obtain the dimensionless continuity equation as

$$\frac{\partial U}{\partial X} + \frac{\partial V}{\partial Y} = 0. \tag{4.14}$$

The dimensional x-momentum equation is re-expressed as

$$\frac{\partial u}{\partial \tilde{t}} + u\frac{\partial u}{\partial x} + v\frac{\partial u}{\partial y} = -\frac{1}{\rho}\frac{\partial p}{\partial x} + \frac{\mu}{\rho}\left(\frac{\partial^2 u}{\partial x^2} + \frac{\partial^2 u}{\partial y^2}\right) - \frac{P_v}{\rho}(u) - \frac{P_i}{\rho}(u^2 + v^2).$$

Introducing the non-dimensional variables:

$$x = LX, \quad y = LY, \quad u = u_0 U, \quad v = u_0 V, \text{ and } \quad t = \frac{L}{u_0}\tilde{t}.$$

Substituting into the dimensional equation:

$$\frac{u_0^2}{L}\frac{\partial U}{\partial t}+\frac{u_0^2}{L}U\frac{\partial U}{\partial X}+\frac{u_0^2}{L}V\frac{\partial U}{\partial Y}=-\frac{1}{\rho}\frac{\partial p}{\partial x}+\frac{\mu}{\rho}\left(\frac{u_0}{L^2}\frac{\partial^2 U}{\partial X^2}+\frac{u_0}{L^2}\frac{\partial^2 U}{\partial Y^2}\right)-\frac{P_v}{\rho}(Uu_0) - \frac{P_i}{\rho}((u_0U)^2+(u_0V)^2)$$

Collecting like coefficient terms

$$\frac{u_0^2}{L}\left(\frac{\partial U}{\partial t}+U\frac{\partial U}{\partial X}+V\frac{\partial U}{\partial Y}\right)=-\frac{1}{\rho}\frac{\partial p}{\partial x}+\frac{\mu u_0}{\rho L^2}\left(\frac{\partial^2 U}{\partial X^2}+\frac{\partial^2 U}{\partial Y^2}\right)-\frac{P_v u_0}{\rho}U - \frac{P_i u_0^2}{\rho}(U^2+V^2) \tag{4.15}$$

Dividing through out (4.15) by $\frac{u_0^2}{L}$:

$$\frac{\partial U}{\partial t}+U\frac{\partial U}{\partial X}+V\frac{\partial U}{\partial Y}=-\frac{L}{u_0^2}\frac{1}{\rho}\frac{\partial p}{\partial x}+\frac{\mu}{L\rho u_0}\left(\frac{\partial^2 U}{\partial X^2}+\frac{\partial^2 U}{\partial Y^2}\right)-\frac{P_v L}{\rho u_0}U - \frac{P_i u_0^2 L}{\rho u_0^2}(U^2+V^2). \tag{4.16}$$

Using the chain rule implies

$$\frac{\partial p}{\partial x}=\frac{\partial p}{\partial X}\cdot\frac{\partial X}{\partial x}=\frac{1}{L}\frac{\partial p}{\partial X}\Rightarrow\frac{\partial p}{\partial x}=\frac{1}{L}\frac{\partial p}{\partial X}. \tag{4.17}$$

Substitute (4.17) into (4.16) gives

$$\frac{\partial U}{\partial t}+U\frac{\partial U}{\partial X}+V\frac{\partial U}{\partial Y}=-\frac{1}{u_0^2}\frac{1}{\rho}\frac{\partial p}{\partial X}+\frac{1}{Re}\left(\frac{\partial^2 U}{\partial X^2}+\frac{\partial^2 U}{\partial Y^2}\right)-Gr_v U - Gr_i(U^2+V^2)$$

The dimensionless numbers $Re,\ Gr_v$, and Gr_i are defined as:

$$Re = \frac{\rho u_0 L}{\mu} \quad \text{(Reynolds number)}, Gr_v \ = \frac{P_v L}{\rho u_0} \quad \text{(viscous resistance parameter)},$$

and

$$Gr_i = \frac{P_i L}{\rho} \quad \text{(inertial resistance parameter)}.$$

Thus, the final dimensionless x-momentum equation is:

$$\frac{\partial U}{\partial t} + U\frac{\partial U}{\partial X} + V\frac{\partial U}{\partial Y} = -\frac{\partial P}{\partial X} + \frac{1}{Re}\left(\frac{\partial^2 U}{\partial X^2} + \frac{\partial^2 U}{\partial Y^2}\right) - Gr_v U - Gr_i(U^2 + V^2). \quad (4.18)$$

Similarly, the dimensionless form of the y-momentum equation can be obtained as follows:

$$\frac{u_o^2}{L}\frac{\partial V}{\partial t} + \frac{u_o^2}{L}U\frac{\partial V}{\partial X} + \frac{u_o^2}{L}V\frac{\partial V}{\partial Y} = -\frac{1}{\rho}\frac{\partial p}{\partial y} + \frac{\mu}{\rho}\left(\frac{u_o}{L^2}\frac{\partial^2 V}{\partial X^2} + \frac{u_o}{L^2}\frac{\partial^2 V}{\partial Y^2}\right) - \frac{P_v}{\rho}v - \frac{P_i}{\rho}(v^2 + u^2).$$

or,

$$\frac{u_o^2}{L}\left[\frac{\partial V}{\partial t} + U\frac{\partial V}{\partial X} + V\frac{\partial V}{\partial Y}\right] = -\frac{1}{\rho}\frac{\partial p}{\partial y} + \frac{\mu}{\rho}\frac{u_o}{L^2}\left(\frac{\partial^2 V}{\partial X^2} + \frac{\partial^2 V}{\partial Y^2}\right) - \frac{P_v u_o V}{\rho} - \frac{P_i}{\rho}\left[(u_o V)^2 + (u_o U)^2\right]$$

$$\Rightarrow \frac{\partial V}{\partial t} + U\frac{\partial V}{\partial X} + V\frac{\partial V}{\partial Y} = -\frac{L}{u_o^2}\frac{1}{\rho}\frac{\partial p}{\partial y} + \frac{L}{u_o^2}\frac{\mu}{\rho}\frac{u_o}{L^2}\left(\frac{\partial^2 V}{\partial X^2} + \frac{\partial^2 V}{\partial Y^2}\right) - \frac{P_v L}{\rho u_o}V - \frac{P_i u_o^2 L}{\rho u_o^2}(V^2 + U^2)$$

$$\Rightarrow \frac{\partial V}{\partial t} + U\frac{\partial V}{\partial X} + V\frac{\partial V}{\partial Y} = -\frac{L}{u_o^2}\frac{1}{\rho}\frac{\partial}{\partial Y}\frac{\partial Y}{\partial y}(p) + \frac{\mu}{\rho L u_o}\left(\frac{\partial^2 V}{\partial X^2} + \frac{\partial^2 V}{\partial Y^2}\right) - Gr_v V - Gr_i(V^2 + U^2)$$

$$\Rightarrow \frac{\partial V}{\partial t} + U\frac{\partial V}{\partial X} + V\frac{\partial V}{\partial Y} = -L\frac{\partial}{\partial Y}\frac{1}{L}\left(\frac{p}{\rho u_o^2}\right) + \frac{1}{\frac{\rho L u_o}{\mu}}\left(\frac{\partial^2 V}{\partial X^2} + \frac{\partial^2 V}{\partial Y^2}\right) - Gr_v V - Gr_i(V^2 + U^2)$$

$$\Rightarrow \frac{\partial V}{\partial t} + U\frac{\partial V}{\partial X} + V\frac{\partial V}{\partial Y} = -\frac{\partial P}{\partial Y} + \frac{1}{Re}\left(\frac{\partial^2 V}{\partial X^2} + \frac{\partial^2 V}{\partial Y^2}\right) - Gr_v V - Gr_i(V^2 + U^2) \tag{4.19}$$

The dimensional energy equation is given by

$$\frac{\partial \tilde{T}}{\partial \tilde{t}} + u\frac{\partial \tilde{T}}{\partial x} + v\frac{\partial \tilde{T}}{\partial y} = \frac{k}{\rho C_p}\left(\frac{\partial^2 \tilde{T}}{\partial x^2} + \frac{\partial^2 \tilde{T}}{\partial y^2}\right) - \frac{1}{\rho C_p}\frac{\partial q_r}{\partial y}. \tag{4.20}$$

Using the non-dimensional variables:

$$x = LX, \quad y = LY, \quad u = u_0 U, \quad v = u_0 V, \quad t = \frac{L}{u_0}\tilde{t} \text{ and } \quad \tilde{T} = T + T_\infty$$

. (4.20) can be transformed into

$$\left(\frac{u_0}{L}\right)\frac{\partial T}{\partial t} + \frac{u_0}{L}U\frac{\partial T}{\partial X} + \frac{u_0}{L}V\frac{\partial T}{\partial Y} = \frac{k}{\rho C_p}\left(\frac{1}{L^2}\frac{\partial^2 T}{\partial X^2} + \frac{1}{L^2}\frac{\partial^2 T}{\partial Y^2}\right) - \frac{1}{\rho C_p}\left(-\frac{16\sigma^*}{3k^*}T^3\frac{\partial T}{\partial y}\right) \tag{4.21}$$

The (4.21), further simplifies to

$$\frac{u_0}{L}\left(\frac{\partial T}{\partial t} + U\frac{\partial T}{\partial X} + V\frac{\partial T}{\partial Y}\right) = \frac{k}{\rho C_p L^2}\left(\frac{\partial^2 T}{\partial X^2} + \frac{\partial^2 T}{\partial Y^2}\right) + \frac{1}{\rho C_p}\cdot\frac{16\sigma^*}{3k^* L^2}T^3\frac{\partial^2 T}{\partial Y^2}.$$

Divide both sides by $\frac{u_0}{L}$; implies

$$\frac{\partial T}{\partial t} + U\frac{\partial T}{\partial X} + V\frac{\partial T}{\partial Y} = \frac{1}{Re\cdot Pr}\left(\frac{\partial^2 T}{\partial X^2} + \frac{\partial^2 T}{\partial Y^2}\right) + \frac{Rd}{Re\cdot Pr}T^3\frac{\partial^2 T}{\partial Y^2}.$$

Where the dimensionless parameters Pr and Rd are given by

$$Pr = \frac{\mu C_p}{k}, \qquad \text{(Prandtl number)}$$

$$Rd = \frac{16\sigma^* T_\infty^3}{3k^* k}, \qquad \text{(Radiation parameter)}$$

Hence, the final dimensionless energy equation becomes

$$\frac{\partial T}{\partial t} + U\frac{\partial T}{\partial X} + V\frac{\partial T}{\partial Y} = \frac{1}{RePr}\left(\frac{\partial^2 T}{\partial X^2} + \frac{\partial^2 T}{\partial Y^2}\right) + \frac{Rd}{RePr}\frac{\partial^2 T}{\partial Y^2}. \tag{4.22}$$

4.5 Dimensionless Governing Equations

The set of transformed dimensionless equations are described as

Continuity Equation:

$$\frac{\partial U}{\partial X} + \frac{\partial V}{\partial Y} = 0. \tag{4.23}$$

X-Component of momentum equation:

$$\frac{\partial U}{\partial t} + U\frac{\partial U}{\partial X} + V\frac{\partial U}{\partial Y} = -\frac{\partial P}{\partial X} + \frac{1}{Re}\left(\frac{\partial^2 U}{\partial X^2} + \frac{\partial^2 U}{\partial Y^2}\right) - Gr_v U - Gr_i(U^2 + V^2). \tag{4.24}$$

Y-Component of momentum equation:

$$\frac{\partial V}{\partial t} + U\frac{\partial V}{\partial X} + V\frac{\partial V}{\partial Y} = -\frac{\partial P}{\partial Y} + \frac{1}{Re}\left(\frac{\partial^2 V}{\partial X^2} + \frac{\partial^2 V}{\partial Y^2}\right) - Gr_v V - Gr_i(V^2 + U^2). \tag{4.25}$$

Energy equation:

$$\frac{\partial T}{\partial t} + U\frac{\partial T}{\partial X} + V\frac{\partial T}{\partial Y} = \frac{1}{RePr}\left(\frac{\partial^2 T}{\partial X^2} + \frac{\partial^2 T}{\partial Y^2}\right) + \frac{Rd}{RePr}\frac{\partial^2 T}{\partial Y^2}. \tag{4.26}$$

The associated conditions for boundaries are given below:

$$U = 1, \quad V = 0 \quad \forall \quad x \in [0,1] \quad \text{and} \quad y = 1 \quad \text{on} \quad \Omega.$$

$$U = V = 0 \quad \forall \quad x \in \{0,1\}, \quad \text{and} \quad y \in [0,1] \quad \text{on} \quad \Omega.$$

$$U = 0, \quad V = 0 \quad \forall \quad x \in [0,1] \quad \text{and} \quad y = 0 \quad \text{on} \quad \Omega.$$

$$U = V = 0 \quad \forall \quad x \in \{0,1\}, \quad \text{and} \quad y \in [0,1] \quad \text{on} \quad \Omega.$$

$$T = 1 \quad \forall \quad x \in [0,1] \quad \text{at} \quad y = 0.$$

$$T = 0 \quad \forall \quad x \in [0,1] \quad \text{and at} \quad y = 1.$$

$$\frac{\partial T}{\partial x} = 0 \quad \forall \quad x \in \{0,1\}, \quad \text{and} \quad y \in [0,1] \quad \text{on} \quad \Omega.$$

The dimensionless parameters given by

$$Re = \frac{\rho u_o L}{\mu}, \quad Rd = \frac{16\sigma^* T^3}{3k^* k}, \quad Pr = \frac{\mu C_p}{k}, \quad Gr_v = \frac{P_v L}{\rho u_0} \quad and \quad Gr_i = \frac{P_i L}{\rho} \quad .$$

In order to transform differential equations in (4.23) - (4.26) into the weak formulation the method applies is the variational method. In this procedure, the PDEs are a suitable test function and then integrates the resulting equation over the whole computational domain. The weak formulation of the strong form of governing PDEs from . (4.23) to (4.26) give below:
The weak form for u-component of momentum equation (4.24) as follows:

$$\frac{\partial U}{\partial t}+U\frac{\partial U}{\partial X}+V\frac{\partial U}{\partial Y} = -\frac{\partial P}{\partial X}+\frac{1}{Re}\left(\frac{\partial^2 U}{\partial X^2}+\frac{\partial^2 U}{\partial Y^2}\right)-Gr_v U-Gr_i(U^2+V^2).$$

Multiplying by test function $\tilde{U}$ first and then integrate over computational domain, implies

$$\frac{\partial U}{\partial t}\tilde{U} + \left[\left(U\frac{\partial U}{\partial X}\right) + \left(V\frac{\partial U}{\partial Y}\right)\right]\tilde{U} - q\frac{\partial U}{\partial X}\tilde{U} = -\frac{\partial P}{\partial X}\tilde{U} + \frac{1}{Re}\left(\frac{\partial^2 U}{\partial X^2} + \frac{\partial^2 U}{\partial Y^2}\right)\tilde{U} - Gr_v U\tilde{U} - Gr_i(U^2+V^2)\tilde{U}. \tag{4.27}$$

$$\frac{\partial U}{\partial t}\tilde{U} + \left[\left(U\frac{\partial U}{\partial X}\right) + \left(V\frac{\partial U}{\partial Y}\right)\right]\tilde{U} - q\frac{\partial}{\partial X}(U\tilde{U}) + qU\frac{\partial \tilde{U}}{\partial X} = -\frac{\partial}{\partial X}(P\tilde{U}) + P\frac{\partial \tilde{U}}{\partial X} + \frac{1}{Re}\left(\frac{\partial^2 U}{\partial X^2} + \frac{\partial^2 U}{\partial Y^2}\right)\tilde{U} - Gr_v U\tilde{U} - Gr_i(U^2+V^2)\tilde{U}.$$

$$\int_{\Omega^n} \frac{\partial U}{\partial t}\tilde{U}d\Omega + \int_{\Omega^n} \Big[U\frac{\partial U}{\partial X} + V\frac{\partial U}{\partial Y}\Big]\tilde{U}d\Omega - q\int_{\Omega^n} \frac{\partial}{\partial X}(U\tilde{U})d\Omega$$
$$+ q\int_{\Omega^n} U\frac{\partial \tilde{U}}{\partial X}d\Omega = -\int_{\Omega^n} \frac{\partial}{\partial X}(P\tilde{U})d\Omega + P\int_{\Omega^n} \frac{\partial \tilde{U}}{\partial X}d\Omega \tag{4.28}$$
$$+ \frac{1}{Re}\int_{\Omega^n} \Big(\frac{\partial^2 U}{\partial X^2} + \frac{\partial^2 U}{\partial Y^2}\Big)\tilde{U}d\Omega - Gr_v\int_{\Omega^n} U\tilde{U}d\Omega - Gr_i\int_{\Omega^n} (U^2+V^2)\tilde{U}d\Omega.$$

Consider,

$$\int_{\Omega^n} \frac{\partial U}{\partial t}\,\tilde{U}\,d\Omega + \int_{\Omega^n} \Big[U\frac{\partial U}{\partial X} + V\frac{\partial U}{\partial Y}\Big]\tilde{U}\,d\Omega = \int_{\Omega^n} \frac{(U^{n+1}-U^n)}{\delta t}\,\tilde{U}\,d\Omega$$
$$+ \int_{\Omega^n} \Big[U\frac{\partial U}{\partial X} + V\frac{\partial U}{\partial Y}\Big]\tilde{U}\,d\Omega.$$

$$\Longrightarrow \int_{\Omega^n} \frac{\partial U}{\partial t}\tilde{U}d\Omega + \int_{\Omega^n} \Big[\Big(U\frac{\partial U}{\partial X}\Big) + \Big(V\frac{\partial U}{\partial Y}\Big)\Big]\tilde{U}d\Omega = \frac{1}{\delta t}\int_{\Omega^n} U^{n+1}\tilde{U}d\Omega$$
$$- \frac{1}{\delta t}\int_{\Omega^n} U^n\tilde{U}d\Omega + \int_{\Omega^n} \Big[\Big(U\frac{\partial U}{\partial X}\Big) + \Big(V\frac{\partial U}{\partial Y}\Big)\Big]\tilde{U}d\Omega.$$

$$\int_{\Omega^n} \frac{\partial U}{\partial t}\tilde{U}d\Omega + \int_{\Omega^n} \Big[\Big(U\frac{\partial U}{\partial X}\Big) + \Big(V\frac{\partial U}{\partial Y}\Big)\Big]\tilde{U}d\Omega = \frac{1}{\delta t}\int_{\Omega^n} U^{n+1}\tilde{U}d\Omega$$
$$- \frac{1}{\delta t}\Big(U^n\ o\ X^n\Big)\tilde{U}d\Omega.$$

$$\Longrightarrow\ \frac{1}{\delta t}\int_{\Omega^n} U^{n+1}\tilde{U}d\Omega - \frac{1}{\delta t}\Big(U^n\ o\ X^n\Big)\tilde{U}d\Omega - q\int_{\Omega^n} \frac{\partial}{\partial X}(U\tilde{U})d\Omega + q\int_{\Omega^n} U\frac{\partial \tilde{U}}{\partial X}d\Omega =$$
$$-\int_{\Omega^n} \frac{\partial}{\partial X}(P\tilde{U})d\Omega + P\int_{\Omega^n} \frac{\partial \tilde{U}}{\partial X}d\Omega + \frac{1}{Re}\int_{\Omega^n} \Big(\frac{\partial^2 U}{\partial X^2} + \frac{\partial^2 U}{\partial Y^2}\Big)\tilde{U}d\Omega - Gr_v\int_{\Omega^n} U\tilde{U}d\Omega$$
$$-Gr_i\int_{\Omega^n} (U^2+V^2)\tilde{U}d\Omega. \tag{4.29}$$

Using Green's theorem for Laplacian term as

$$\int_{\Omega} \psi \Delta\phi \; d\Omega = -\int_{\Omega} \nabla\phi \nabla\psi \; d\Omega + \int_{\Omega} \psi(\nabla\phi n) \; d\Gamma.$$

Here,

$$\psi = \tilde{U}, \; \Delta\phi = \frac{\partial^2 U}{\partial X^2}, \; \Delta\phi = \frac{\partial^2 U}{\partial Y^2}, \; \nabla\phi = \frac{\partial U}{\partial X}, \; \nabla\phi = \frac{\partial U}{\partial Y}, \; \nabla\psi = \frac{\partial \tilde{U}}{\partial X}, \; \nabla\psi = \frac{\partial \tilde{U}}{\partial Y}.$$

As,

$$\nabla\phi n = \frac{\partial \phi}{\partial n} = n_x \frac{\partial \phi}{\partial X} + n_y \frac{\partial \phi}{\partial Y} \qquad (\phi = U).$$

$$\int_{\Omega^n} \left(\frac{\partial^2 U}{\partial X^2} + \frac{\partial^2 U}{\partial Y^2} \right) \tilde{U} \, d\Omega = -\int_{\Omega^n} \frac{\partial U}{\partial X} \frac{\partial \tilde{U}}{\partial X} \, d\Omega + \oint_{\Gamma} \tilde{U} \left(n_x \frac{\partial U}{\partial X} \right) d\Gamma$$
$$- \int_{\Omega^n} \frac{\partial U}{\partial Y} \frac{\partial \tilde{U}}{\partial Y} \, d\Omega + \oint_{\Gamma} \tilde{U} \left(n_y \frac{\partial U}{\partial Y} \right) d\Gamma.$$

Now, (4.29) becomes

$$\frac{1}{\delta t} \int_{\Omega^n} U^{n+1} \tilde{U} d\Omega - \frac{1}{\delta t} \left(U^n \; o \; X^n \right) \tilde{U} d\Omega - q \int_{\Omega^n} \frac{\partial}{\partial X} (U\tilde{U}) d\Omega \; (\to 0) + q \int_{\Omega^n} U \frac{\partial \tilde{U}}{\partial X} d\Omega =$$

$$- \int_{\Omega^n} \frac{\partial}{\partial X} (P\tilde{U}) d\Omega \; (\to 0) + P \int_{\Omega^n} \frac{\partial \tilde{U}}{\partial X} d\Omega - \frac{1}{Re} \int_{\Omega^n} \frac{\partial U}{\partial X} \frac{\partial \tilde{U}}{\partial X} d\Omega + \frac{1}{Re} \oint_{\Gamma} \tilde{U} \left(n_x \frac{\partial U}{\partial X} \right) d\Gamma$$
$$- \frac{1}{Re} \int_{\Omega^n} \frac{\partial U}{\partial Y} \frac{\partial \tilde{U}}{\partial Y} d\Omega + \frac{1}{Re} \oint_{\Gamma} \tilde{U} \left(n_y \frac{\partial U}{\partial Y} \right) d\Gamma - Gr_v \int_{\Omega^n} U \tilde{U} d\Omega$$

$$- Gr_i \int_{\Omega^n} (U^2 + V^2) \tilde{U} d\Omega.$$

$$\implies \frac{1}{\delta t}\int_{\Omega^n} U^{n+1}\tilde{U}d\Omega - \frac{1}{\delta t}\Big(U^n \; o \; X^n\Big)\tilde{U}d\Omega + q\int_{\Omega^n} U\frac{\partial \tilde{U}}{\partial X}d\Omega = P\int_{\Omega^n}\frac{\partial \tilde{U}}{\partial X}d\Omega$$
$$-\frac{1}{Re}\int_{\Omega^n}\frac{\partial U}{\partial X}\frac{\partial \tilde{U}}{\partial X}d\Omega + \frac{1}{Re}\oint_{\Gamma}\tilde{U}\Big(n_x\frac{\partial U}{\partial X}\Big)d\Gamma - \frac{1}{Re}\int_{\Omega^n}\frac{\partial U}{\partial Y}\frac{\partial \tilde{U}}{\partial Y}d\Omega +$$
$$\frac{1}{Re}\oint_{\Gamma}\tilde{U}\Big(n_y\frac{\partial U}{\partial Y}\Big)d\Gamma - Gr_v\int_{\Omega^n} U\tilde{U}d\Omega - Gr_i\int_{\Omega^n}(U^2+V^2)\tilde{U}d\Omega.$$

Taking domain at current time step, we can write

$$\frac{1}{\delta t}\int_{\Omega^n} U^{n+1}\tilde{U}d\Omega - \frac{1}{\delta t}\Big(U^n \; o \; X^n\Big)\tilde{U}d\Omega + q^{n+1}\int_{\Omega^{n+1}} U^{n+1}\frac{\partial \tilde{U}}{\partial X^{n+1}}d\Omega$$
$$= P^{n+1}\int_{\Omega^{n+1}}\frac{\partial \tilde{U}}{\partial X^{n+1}}d\Omega - \frac{1}{Re}\int_{\Omega^{n+1}}\frac{\partial U^{n+1}}{\partial X^{n+1}}\frac{\partial \tilde{U}}{\partial X^{n+1}}d\Omega + \frac{1}{Re}\oint_{\Gamma}\tilde{U}\Big(n_x\frac{\partial U^{n+1}}{\partial X^{n+1}}\Big)d\Gamma$$
$$-\frac{1}{Re}\int_{\Omega^{n+1}}\frac{\partial U^{n+1}}{\partial Y^{n+1}}\frac{\partial \tilde{U}}{\partial Y}d\Omega + \frac{1}{Re}\oint_{\Gamma}\tilde{U}\Big(n_y\frac{\partial U^{n+1}}{\partial Y^{n+1}}\Big)d\Gamma - Gr_v\int_{\Omega^{n+1}} U^{n+1}\tilde{U}d\Omega$$
$$- Gr_i\int_{\Omega^{n+1}}(U^{2n+2}+V^{2n+2})\tilde{U}d\Omega. \tag{4.30}$$

(4.30) is weak form of X-component of momentum equation.

Similarly, the weak form for Y-component of momentum equation (4.25) given below:

$$\frac{1}{\delta t}\int_{\Omega^n} V^{n+1}\tilde{V}d\Omega - \frac{1}{\delta t}\Big(V^n \; o \; X^n\Big)\tilde{V}d\Omega + q^{n+1}\int_{\Omega^{n+1}} V^{n+1}\frac{\partial \tilde{V}}{\partial Y^{n+1}}d\Omega$$
$$= P^{n+1}\int_{\Omega^{n+1}}\frac{\partial \tilde{V}}{\partial Y^{n+1}}d\Omega - \frac{1}{Re}\int_{\Omega^{n+1}}\frac{\partial V^{n+1}}{\partial X^{n+1}}\frac{\partial \tilde{V}}{\partial X^{n+1}}d\Omega + \oint_{\Gamma}\tilde{V}\Big(n_x\frac{\partial V^{n+1}}{\partial X^{n+1}}\Big)d\Gamma -$$
$$\frac{1}{Re}\int_{\Omega^{n+1}}\frac{\partial V^{n+1}}{\partial Y^{n+1}}\frac{\partial \tilde{V}}{\partial Y}d\Omega + \frac{1}{Re}\oint_{\Gamma}\tilde{V}\Big(n_y\frac{\partial V^{n+1}}{\partial Y^{n+1}}\Big)d\Gamma - Gr_v\int_{\Omega^{n+1}} V^{n+1}\tilde{V}d\Omega$$
$$- Gr_i\int_{\Omega^{n+1}}(V^{2n+2}+U^{2n+2})\tilde{V}d\Omega. \tag{4.31}$$

equation (4.31) is weak form of Y-component of momentum equation.

The energy equation (4.26) stated below

$$\frac{\partial T}{\partial t}+U\frac{\partial T}{\partial X}+V\frac{\partial T}{\partial Y}=\frac{1}{RePr}\left(\frac{\partial^2 T}{\partial X^2}+\frac{\partial^2 T}{\partial Y^2}\right)+\frac{Rd}{RePr}\frac{\partial^2 T}{\partial Y^2}, \tag{4.32}$$

is transformed into weak form as follows.

Multiplying (4.32) by test function $\tilde{T}$ first and then integrate over computational domain, implies

$$\frac{\partial T}{\partial t}\tilde{T}+\left[\left(U\frac{\partial T}{\partial X}\right)+\left(V\frac{\partial T}{\partial Y}\right)\right]\tilde{T}=\frac{1}{RePr}\left(\frac{\partial^2 T}{\partial X^2}+\frac{\partial^2 T}{\partial Y^2}\right)\tilde{T}+\frac{Rd}{RePr}\frac{\partial^2 T}{\partial Y^2}\tilde{T}$$

$$\int_{\Omega^n}\frac{\partial T}{\partial t}\tilde{T}d\Omega+\int_{\Omega^n}\left[\left(U\frac{\partial T}{\partial X}\right)+\left(V\frac{\partial T}{\partial Y}\right)\right]\tilde{T}d\Omega=\frac{1}{RePr}\int_{\Omega^n}\left(\frac{\partial^2 T}{\partial X^2}+\frac{\partial^2 T}{\partial Y^2}\right)\tilde{T}d\Omega$$
$$+\frac{Rd}{RePr}\int_{\Omega^n}\frac{\partial^2 T}{\partial Y^2}\tilde{T}d\Omega. \tag{4.33}$$

$$\int_{\Omega^n}\frac{\partial T}{\partial t}\tilde{T}d\Omega+\int_{\Omega^n}\left[U\frac{\partial T}{\partial X}+V\frac{\partial T}{\partial Y}\right]\tilde{T}d\Omega=\int_{\Omega^n}\frac{(T^{n+1}-T^n)}{\delta t}\tilde{T}d\Omega$$
$$+\int_{\Omega^n}\left[U\frac{\partial T}{\partial X}+V\frac{\partial T}{\partial Y}\right]\tilde{T}d\Omega$$
$$=\frac{1}{\delta t}\int_{\Omega^n}T^{n+1}\tilde{T}d\Omega-\frac{1}{\delta t}\int_{\Omega^n}T^n\tilde{T}d\Omega+\int_{\Omega^n}\left[U\frac{\partial T}{\partial X}+V\frac{\partial T}{\partial Y}\right]\tilde{T}d\Omega$$

$\Longrightarrow$

$$\int_{\Omega^n}\frac{\partial T}{\partial t}\tilde{T}d\Omega+\int_{\Omega^n}\left[U\frac{\partial T}{\partial X}+V\frac{\partial T}{\partial Y}\right]\tilde{T}d\Omega=\frac{1}{\delta t}\int_{\Omega^n}T^{n+1}\tilde{T}d\Omega-\frac{1}{\delta t}\left(T^n\ o\ X^n\right)\tilde{T}d\Omega$$

$$\frac{1}{\delta t}\int_{\Omega^n}T^{n+1}\tilde{T}\,d\Omega-\frac{1}{\delta t}(T^n\ o\ X^n)\tilde{T}\,d\Omega=\frac{1}{RePr}\int_{\Omega^n}\left(\frac{\partial^2 T}{\partial X^2}+\frac{\partial^2 T}{\partial Y^2}\right)\tilde{T}\,d\Omega$$
$$+\frac{Rd}{RePr}\int_{\Omega^n}\frac{\partial^2 T}{\partial Y^2}\tilde{T}\,d\Omega \tag{4.34}$$

Using Green's theorem for Laplacian term as

$$\int_{\Omega} \psi \Delta\phi \; d\Omega = -\int_{\Omega} \nabla\phi \nabla\psi \; d\Omega + \int_{\Omega} \psi(\nabla\phi n) \; d\Gamma.$$

Here,

$$\psi = \tilde{T}, \; \Delta\phi = \frac{\partial^2 T}{\partial X^2}, \; \Delta\phi = \frac{\partial^2 T}{\partial Y^2}, \; \nabla\phi = \frac{\partial T}{\partial X}, \; \nabla\phi = \frac{\partial T}{\partial Y}, \; \nabla\psi = \frac{\partial \tilde{T}}{\partial X}, \; \nabla\psi = \frac{\partial \tilde{T}}{\partial Y} \tag{4.35}$$

As,

$$\nabla\phi n = \frac{\partial \phi}{\partial n} = n_x \frac{\partial \phi}{\partial X} + n_y \frac{\partial \phi}{\partial Y} \qquad (\phi = T).$$

$$\int_{\Omega^n} \left(\frac{\partial^2 T}{\partial X^2} + \frac{\partial^2 T}{\partial Y^2} \right) \tilde{T} d\Omega = -\int_{\Omega^n} \frac{\partial T}{\partial X} \frac{\partial \tilde{T}}{\partial X} d\Omega + \oint_{\Gamma} \tilde{T} \left(n_x \frac{\partial T}{\partial X} \right) d\Gamma - \int_{\Omega^n} \frac{\partial T}{\partial Y} \frac{\partial \tilde{T}}{\partial Y} d\Omega + \oint_{\Gamma} \tilde{T} \left(n_y \frac{\partial T}{\partial Y} \right) d\Gamma.$$

Now (4.34) becomes as

$$\frac{1}{\delta t} \int_{\Omega^n} T^{n+1} \tilde{T} \, d\Omega - \frac{1}{\delta t} \left(T^n \; o \; X^n \right) \tilde{T} \, d\Omega = -\frac{1}{RePr} \int_{\Omega^n} \frac{\partial T}{\partial X} \frac{\partial \tilde{T}}{\partial X} \, d\Omega + \frac{1}{RePr} \oint_{\Gamma} \tilde{T} \left(n_x \frac{\partial T}{\partial X} \right) d\Gamma - \frac{1}{RePr} \int_{\Omega^n} \frac{\partial T}{\partial Y} \frac{\partial \tilde{T}}{\partial Y} \, d\Omega + \frac{1}{RePr} \oint_{\Gamma} \tilde{T} \left(n_y \frac{\partial T}{\partial Y} \right) d\Gamma - \frac{Rd}{RePr} \int_{\Omega^n} \frac{\partial T}{\partial Y} \frac{\partial \tilde{T}}{\partial Y} \, d\Omega + \frac{Rd}{RePr} \oint_{\Gamma} \tilde{T} \left(n_y \frac{\partial T}{\partial Y} \right) d\Gamma.$$

Taking domain at the current time step, we can write

$$\begin{aligned}
&\frac{1}{\delta t}\int\limits_{\Omega^{n+1}} T^{n+1}\tilde{T}\,d\Omega - \frac{1}{\delta t}\big(T^n\ o\ X^n\big)\tilde{T}\,d\Omega \\
&= -\frac{1}{RePr}\int\limits_{\Omega^{n+1}} \frac{\partial T^{n+1}}{\partial X^{n+1}}\frac{\partial \tilde{T}}{\partial X^{n+1}}\,d\Omega + \frac{1}{RePr}\oint\limits_{\Gamma}\tilde{T}\left(n_x\frac{\partial T^{n+1}}{\partial X^{n+1}}\right)\,d\Gamma \\
&\quad - \frac{1}{RePr}\int\limits_{\Omega^{n+1}} \frac{\partial T^{n+1}}{\partial Y^{n+1}}\frac{\partial \tilde{T}}{\partial Y^{n+1}}\,d\Omega + \frac{1}{RePr}\oint\limits_{\Gamma}\tilde{T}\left(n_y\frac{\partial T^{n+1}}{\partial Y^{n+1}}\right)\,d\Gamma \\
&\quad - \frac{Rd}{RePr}\int\limits_{\Omega^{n+1}} \frac{\partial T^{n+1}}{\partial Y^{n+1}}\frac{\partial \tilde{T}}{\partial Y^{n+1}}\,d\Omega + \frac{Rd}{RePr}\oint\limits_{\Gamma}\tilde{T}\left(n_y\frac{\partial T^{n+1}}{\partial Y^{n+1}}\right)\,d\Gamma.
\end{aligned} \tag{4.36}$$

(4.36) is weak form of the energy equation. The weak form of the problem reads:

Find $(U,\ V,\ T)\in$W *and* P$\in$Q such that

$$\begin{aligned}
&\frac{1}{\delta t}\int\limits_{\Omega^n} U^{n+1}\tilde{U}d\Omega - \frac{1}{\delta t}\left(U^n o\ X^n\right)\tilde{U}d\Omega + q^{n+1}\int\limits_{\Omega^{n+1}} U^{n+1}\frac{\partial\tilde{U}}{\partial X^{n+1}}d\Omega = {}_{P^{n+1}}\int\limits_{\Omega^{n+1}}\frac{\partial\tilde{U}}{\partial X^{n+1}}d\Omega \\
&-\frac{1}{Re}\int\limits_{\Omega^{n+1}}\frac{\partial U^{n+1}}{\partial X^{n+1}}\frac{\partial\tilde{U}}{\partial X^{n+1}}d\Omega + \frac{1}{Re}\oint\limits_{\Gamma}\tilde{U}\left(n_x\frac{\partial U^{n+1}}{\partial X^{n+1}}\right)d\Gamma - \frac{1}{Re}\int\limits_{\Omega^{n+1}}\frac{\partial U^{n+1}}{\partial Y^{n+1}}\frac{\partial\tilde{U}}{\partial Y}d\Omega \\
&+\frac{1}{Re}\oint\limits_{\Gamma}\tilde{U}\left(n_y\frac{\partial U^{n+1}}{\partial Y^{n+1}}\right)d\Gamma - Gr_v\int\limits_{\Omega^{n+1}} U^{n+1}\tilde{U}d\Omega - Gr_i\int\limits_{\Omega^{n+1}}(U^{2n+2}+V^{2n+2})\tilde{U}d\Omega,
\end{aligned} \tag{4.37}$$

$$\begin{aligned}
&\frac{1}{\delta t}\int\limits_{\Omega^n} V^{n+1}\tilde{V}d\Omega - \frac{1}{\delta t}\left(V^n o\ X^n\right)\tilde{V}d\Omega + q^{n+1}\int\limits_{\Omega^{n+1}} V^{n+1}\frac{\partial\tilde{V}}{\partial Y^{n+1}}d\Omega \\
&= P^{n+1}\int\limits_{\Omega^{n+1}}\frac{\partial\tilde{V}}{\partial Y^{n+1}}d\Omega - \frac{1}{Re}\int\limits_{\Omega^{n+1}}\frac{\partial V^{n+1}}{\partial X^{n+1}}\frac{\partial\tilde{V}}{\partial X^{n+1}}d\Omega + \frac{1}{Re}\oint\limits_{\Gamma}\tilde{V}\left(n_x\frac{\partial V^{n+1}}{\partial X^{n+1}}\right)d\Gamma \\
&- \frac{1}{Re}\int\limits_{\Omega^{n+1}}\frac{\partial V^{n+1}}{\partial Y^{n+1}}\frac{\partial\tilde{V}}{\partial Y}d\Omega + \frac{1}{Re}\oint\limits_{\Gamma}\tilde{V}\left(n_y\frac{\partial V^{n+1}}{\partial Y^{n+1}}\right)d\Gamma - Gr_v\int\limits_{\Omega^{n+1}} V^{n+1}\tilde{V}d\Omega \\
&- Gr_i\int\limits_{\Omega^{n+1}}(V^{2n+2}+U^{2n+2})\tilde{V}d\Omega,
\end{aligned} \tag{4.38}$$

and

$$\frac{1}{\delta t}\int\limits_{\Omega^{n+1}} T^{n+1}\tilde{T}d\Omega - \frac{1}{\delta t}\Big(T^n\ o\ X^n\Big)\tilde{T}d\Omega = -\frac{1}{RePr}\int\limits_{\Omega^{n+1}} \frac{\partial T^{n+1}}{\partial X^{n+1}}\frac{\partial \tilde{T}}{\partial X^{n+1}}d\Omega$$

$$+\frac{1}{RePr}\oint\limits_{\Gamma}\tilde{T}\Big(n_x\frac{\partial T^{n+1}}{\partial X^{n+1}}\Big)d\Gamma - \frac{1}{RePr}\int\limits_{\Omega^{n+1}}\frac{\partial T^{n+1}}{\partial Y^{n+1}}\frac{\partial \tilde{T}}{\partial Y^{n+1}}d\Omega$$

$$+\frac{1}{RePr}\oint\limits_{\Gamma}\tilde{T}\Big(n_y\frac{\partial T^{n+1}}{\partial Y^{n+1}}\Big)d\Gamma - \frac{Rd}{RePr}\int\limits_{\Omega^{n+1}}\frac{\partial T^{n+1}}{\partial Y^{n+1}}\frac{\partial \tilde{T}}{\partial Y^{n+1}}d \tag{4.39}$$

$$a+\frac{Rd}{RePr}\oint\limits_{\Gamma}\tilde{T}\Big(n_y\frac{\partial T^{n+1}}{\partial Y^{n+1}}\Big)d\Gamma.$$

For all $\tilde{U}$, $\tilde{V}$, $\tilde{T}\in \mathrm{W}$ and $P\in \mathrm{Q}$, where W and Q are the suitable function spaces.

Let $U\approx U_h$, $V\approx V_h$, $T\approx T_h$ and $P\approx P_h$ .with $\mathrm{W}\approx \mathrm{W}_h$ and $\mathrm{Q}\approx \mathrm{Q}_h$,

then the discrete form of the weak problem in (4.37) - (4.39) reads.

Find $(U_h,\ V_h,\ T_h)\in \mathrm{W}_h$ and $P_h\in \mathrm{Q}_h$ such that

$$\frac{1}{\delta t}\int\limits_{\Omega^n} U_h^{n+1}\tilde{U}_h d\Omega - \frac{1}{\delta t}\Big(U_h^n o\ X^n\Big)\tilde{U}_h d\Omega + q_h^{n+1}\int\limits_{\Omega^{n+1}} U_h^{n+1}\frac{\partial \tilde{U}_h}{\partial X^{n+1}}d\Omega$$

$$= P_h^{n+1}\int\limits_{\Omega^{n+1}}\frac{\partial \tilde{U}_h}{\partial X^{n+1}}d\Omega - \frac{1}{Re}\int\limits_{\Omega^{n+1}}\frac{\partial U_h^{n+1}}{\partial X^{n+1}}\frac{\partial \tilde{U}_h}{\partial X^{n+1}}d\Omega + \frac{1}{Re}\oint\limits_{\Gamma}\tilde{U}_h\Big(n_x\frac{\partial U_h^{n+1}}{\partial X^{n+1}}\Big)d\Gamma$$

$$-\frac{1}{Re}\int\limits_{\Omega^{n+1}}\frac{\partial U_h^{n+1}}{\partial Y^{n+1}}\frac{\partial \tilde{U}_h}{\partial Y}d\Omega + \frac{1}{Re}\oint\limits_{\Gamma}\tilde{U}_h\Big(n_y\frac{\partial U_h^{n+1}}{\partial Y^{n+1}}\Big)d\Gamma - Gr_v\int\limits_{\Omega^{n+1}} U_h^{n+1}\tilde{U}_h d\Omega$$
$$-Gr_i\int\limits_{\Omega^{n+1}}(U_h^{2n+2}+V_h^{2n+2})\tilde{U}_h d\Omega, \tag{4.40}$$

$$\frac{1}{\delta t}\int\limits_{\Omega^n} V_h^{n+1}\tilde{V}_h d\Omega - \frac{1}{\delta t}\Big(V_h^n o\ X^n\Big)\tilde{V}_h d\Omega + q_h^{n+1}\int\limits_{\Omega^{n+1}} V_h^{n+1}\frac{\partial \tilde{V}_h}{\partial Y^{n+1}}d\Omega = P_h^{n+1}$$
$$\int\limits_{\Omega^{n+1}} \frac{\partial \tilde{V}_h}{\partial Y^{n+1}}d\Omega - \frac{1}{Re}\int\limits_{\Omega^{n+1}} \frac{\partial V_h^{n+1}}{\partial X^{n+1}}\frac{\partial \tilde{V}_h}{\partial X^{n+1}}d\Omega + \frac{1}{Re}\oint\limits_{\Gamma}\tilde{V}_h\Big(n_x\frac{\partial V_h^{n+1}}{\partial X^{n+1}}\Big)d\Gamma$$
$$-\frac{1}{Re}\int\limits_{\Omega^{n+1}} \frac{\partial V_h^{n+1}}{\partial Y^{n+1}}\frac{\partial \tilde{V}_h}{\partial Y}d\Omega + \frac{1}{Re}\oint\limits_{\Gamma}\tilde{V}_h\Big(n_y\frac{\partial V_h^{n+1}}{\partial Y^{n+1}}\Big)d\Gamma - Gr_v\int\limits_{\Omega^{n+1}} V_h^{n+1}\tilde{V}_h d\Omega$$
$$-Gr_i\int\limits_{\Omega^{n+1}}(V_h^{2n+2}+U_h^{2n+2})\tilde{V}_h d\Omega, \tag{4.41}$$

and

$$\frac{1}{\delta t}\int\limits_{\Omega^{n+1}} T_h^{n+1}\tilde{T}_h d\Omega - \frac{1}{\delta t}\Big(T_h^n\ o\ X^n\Big)\tilde{T}_h d\Omega = -\frac{1}{RePr}\int\limits_{\Omega^{n+1}} \frac{\partial T_h^{n+1}}{\partial X^{n+1}}\frac{\partial \tilde{T}_h}{\partial X^{n+1}}d\Omega$$
$$+\frac{1}{RePr}\oint\limits_{\Gamma}\tilde{T}_h\Big(n_x\frac{\partial T_h^{n+1}}{\partial X^{n+1}}\Big)d\Gamma - \frac{1}{RePr}\int\limits_{\Omega^{n+1}} \frac{\partial T_h^{n+1}}{\partial Y^{n+1}}\frac{\partial \tilde{T}_h}{\partial Y^{n+1}}d\Omega$$
$$+\frac{1}{RePr}\oint\limits_{\Gamma}\tilde{T}_h\Big(n_y\frac{\partial T_h^{n+1}}{\partial Y^{n+1}}\Big)d\Gamma - \frac{Rd}{RePr}\int\limits_{\Omega^{n+1}} \frac{\partial T_h^{n+1}}{\partial Y^{n+1}}\frac{\partial \tilde{T}_h}{\partial Y^{n+1}}d\Omega$$
$$+\frac{Rd}{RePr}\oint\limits_{\Gamma}\tilde{T}_h\Big(n_y\frac{\partial T_h^{n+1}}{\partial Y^{n+1}}\Big)d\Gamma. \tag{4.42}$$

FEM approximation is achieved by using the approximate trial solution functions and trial test functions.

These functions are the linear combination of nodal unknowns and shape functions which are linearly independent. Given below are the trial solution functions:

$$U_h = \sum_{j=1}^{m} U_j\xi_j, \qquad V_h = \sum_{j=1}^{m} V_j\xi_j, \qquad T_h = \sum_{j=1}^{m} T_j\xi_j, \qquad P_h = \sum_{j=1}^{l} P_j\eta_j.$$

Similarly, following trial approximated functions are defined for test spaces:

$$(\tilde{U}_h,\ \tilde{V}_h,\ \tilde{T}_h) = \sum_{i=1}^{m}(\tilde{U}_i,\ \tilde{V}_i,\ \tilde{T}_i)\xi_i.$$

The Eqs. (4.40) to (4.42), weak formulation can be expressed as

(4.40)⇒

$$\begin{aligned}
&\frac{1}{\delta t}\int\limits_{\Omega^n}\left(\sum_{j=1}^{m}U_j\xi_j\right)^{n+1}\sum_{i=1}^{m}\tilde{U}_i\xi_i d\Omega-\frac{1}{\delta t}\left(\left(\sum_{j=1}^{m}U_j\xi_j\right)^{n} o\ X^n\right)\sum_{i=1}^{m}\tilde{U}_i\xi_i d\Omega\\
&+\sum_{i=1}^{l}q_i\xi_j\int\limits_{\Omega^n}\sum_{j=1}^{m}U_j\xi_j\frac{\partial}{\partial X}\sum_{i=1}^{m}\tilde{U}_i\xi_i d\Omega=\sum_{j=1}^{l}P_j\eta_j\int\limits_{\Omega^n}\frac{\partial}{\partial X}\sum_{i=1}^{m}\tilde{U}_i\xi_i d\Omega\\
&-\frac{1}{Re}\int\limits_{\Omega^n}\frac{\partial}{\partial X}\sum_{j=1}^{m}U_j\xi_j\frac{\partial}{\partial X}\sum_{i=1}^{m}\tilde{U}_i\xi_i d\Omega+\frac{1}{Re}\oint\limits_{\Gamma}\sum_{i=1}^{m}\tilde{U}_i\xi_i\left(n_x\frac{\partial}{\partial X}\sum_{j=1}^{m}U_j\xi_j\right)d\Gamma\\
&-\frac{1}{Re}\int\limits_{\Omega^n}\frac{\partial}{\partial Y}\sum_{j=1}^{m}U_j\xi_j\frac{\partial}{\partial Y}\sum_{i=1}^{m}\tilde{U}_i\xi_i d\Omega+\frac{1}{Re}\oint\limits_{\Gamma}\sum_{i=1}^{m}\tilde{U}_i\xi_i\left(n_y\frac{\partial}{\partial Y}\sum_{j=1}^{m}U_j\xi_j\right)d\Gamma\\
&-Gr_v\int\limits_{\Omega^n}\sum_{j=1}^{m}U_j\xi_j\sum_{i=1}^{m}\tilde{U}_i\xi_i d\Omega-Gr_i\int\limits_{\Omega^n}\left(\left(\sum_{j=1}^{m}U_j\xi_j\right)^{2n+2}\right.\\
&\left.+\left(\sum_{j=1}^{m}V_j\xi_j\right)^{2n+2}\right)\sum_{i=1}^{m}\tilde{U}_i\xi_i d\Omega
\end{aligned}\tag{4.43}$$

By Galerkin's approximation

$$\tilde{U}_h=\sum_{i=1}^{m}\tilde{U}_i\xi_i$$

(4.43), implies

$$\begin{aligned}
&\frac{1}{\delta t}\int\limits_{\Omega^n}\left(\sum_{j=1}^{m}U_j\xi_j\right)^{n+1}\sum_{i=1}^{m}\xi_i d\Omega-\frac{1}{\delta t}\left(\left(\sum_{j=1}^{m}U_j\xi_j\right)^{n} o\ X^n\right)\sum_{i=1}^{m}\xi_i d\Omega\\
&+\sum_{i=1}^{l}q_i\xi_j\int\limits_{\Omega^n}\sum_{j=1}^{m}U_j\xi_j\frac{\partial}{\partial X}\sum_{i=1}^{m}\xi_i d\Omega=\sum_{j=1}^{l}P_j\eta_j\int\limits_{\Omega^n}\frac{\partial}{\partial X}\sum_{i=1}^{m}\xi_i d\Omega\\
&-\frac{1}{Re}\int\limits_{\Omega^n}\frac{\partial}{\partial X}\sum_{j=1}^{m}U_j\xi_j\frac{\partial}{\partial X}\sum_{i=1}^{m}\xi_i d\Omega+\frac{1}{Re}\oint\limits_{\Gamma}\sum_{i=1}^{m}\xi_i\left(n_x\frac{\partial}{\partial X}\sum_{j=1}^{m}U_j\xi_j\right)d\Gamma\\
&-\frac{1}{Re}\int\limits_{\Omega^n}\frac{\partial}{\partial Y}\sum_{j=1}^{m}U_j\xi_j\frac{\partial}{\partial Y}\sum_{i=1}^{m}\xi_i d\Omega+\frac{1}{Re}\oint\limits_{\Gamma}\sum_{i=1}^{m}\xi_i\left(n_y\frac{\partial}{\partial Y}\sum_{j=1}^{m}U_j\xi_j\right)d\Gamma\\
&-Gr_v\int\limits_{\Omega^n}\sum_{j=1}^{m}U_j\xi_j\sum_{i=1}^{m}\xi_i d\Omega-Gr_i\int\limits_{\Omega^n}\left(\left(\sum_{j=1}^{m}U_j\xi_j\right)^{2n+2}\right.\\
&\left.+\left(\sum_{j=1}^{m}V_j\xi_j\right)^{2n+2}\right)\sum_{i=1}^{m}\tilde{U}_i\xi_i d\Omega
\end{aligned}$$

$$\frac{1}{\delta t}\int\limits_{\Omega^n}\Big(\sum_{j=1}^{m}U_j\xi_j\Big)^{n+1}\sum_{i=1}^{m}\xi_i d\Omega-\frac{1}{\delta t}\Big(\Big(\sum_{j=1}^{m}U_j\xi_j\Big)^{n}o\ X^n\Big)\sum_{i=1}^{m}\xi_i d\Omega$$
$$+\sum_{i=1}^{l}q_i\xi_j\int\limits_{\Omega^n}\sum_{j=1}^{m}U_j\xi_j\sum_{i=1}^{m}\frac{\partial\xi_i}{\partial X}d\Omega=\sum_{j=1}^{l}P_j\eta_j\int\limits_{\Omega^n}\sum_{i=1}^{m}\frac{\partial\xi_i}{\partial X}d\Omega$$
$$-\frac{1}{Re}\int\limits_{\Omega^n}\sum_{j=1}^{m}\frac{\partial\xi_j}{\partial X}U_j\sum_{i=1}^{m}\frac{\partial\xi_i}{\partial X}d\Omega+\frac{1}{Re}\oint\limits_{\Gamma}\sum_{i=1}^{m}\xi_i\Big(n_x\sum_{j=1}^{m}\frac{\partial\xi_j}{\partial X}U_j\Big)d\Gamma$$
$$-\frac{1}{Re}\int\limits_{\Omega^n}\sum_{j=1}^{m}\frac{\partial\xi_j}{\partial Y}U_j\sum_{i=1}^{m}\frac{\partial\xi_i}{\partial Y}d\Omega+\frac{1}{Re}\oint\limits_{\Gamma}\sum_{i=1}^{m}\xi_i\Big(n_y\sum_{j=1}^{m}\frac{\partial\xi_j}{\partial Y}U_j\Big)d\Gamma$$
$$-Gr_v\int\limits_{\Omega^n}\sum_{j=1}^{m}U_j\xi_j\sum_{i=1}^{m}\xi_i d\Omega-Gr_i\int\limits_{\Omega^n}\Big(\Big(\sum_{j=1}^{m}U_j\xi_j\Big)^{2n+2}$$
$$+\Big(\sum_{j=1}^{m}V_j\xi_j\Big)^{2n+2}\Big)\sum_{i=1}^{m}\xi_i d\Omega.$$

$\Longrightarrow$

$$\frac{1}{\delta t}\int\limits_{\Omega^n}\Big(U_j\xi_j\Big)^{n+1}\xi_i d\Omega-\frac{1}{\delta t}\Big(\Big(U_j\xi_j\Big)^{n}o\ X^n\Big)\xi_i d\Omega+q_i\xi_j\int\limits_{\Omega^n}U_j\xi_j\frac{\partial\xi_i}{\partial X}d\Omega$$
$$=\eta_j\int\limits_{\Omega^n}\frac{\partial\xi_i}{\partial X}d\Omega-\frac{1}{Re}\int\limits_{\Omega^n}\frac{\partial\xi_j}{\partial X}\frac{\partial\xi_i}{\partial X}d\Omega+\frac{1}{Re}\oint\limits_{\Gamma}\xi_i\Big(n_x\frac{\partial\xi_j}{\partial X}\Big)d\Gamma-\frac{1}{Re}\int\limits_{\Omega^n}\frac{\partial\xi_j}{\partial Y}\frac{\partial\xi_i}{\partial Y}d\Omega+$$
$$\frac{1}{Re}\oint\limits_{\Gamma}\xi_i\Big(n_y\frac{\partial\xi_j}{\partial Y}\Big)d\Gamma-Gr_v\int\limits_{\Omega^n}U_j\xi_j\xi_i d\Omega-Gr_i\int\limits_{\Omega^n}\Big(\Big(U_j\xi_j\Big)^{2n+2}$$
$$+\Big(V_j\xi_j\Big)^{2n+2}\Big)\sum_{i=1}^{m}\xi_i d\Omega.$$

$\Longrightarrow$

$$\frac{1}{\delta t}\int\limits_{\Omega^{n+1}}U_j^{n+1}\xi_j^{n+1}\xi_i^{n+1}d\Omega-\frac{1}{\delta t}\Big(U_j^n\xi_j^n o\ X^n\Big)\xi_i^{n+1}d\Omega+\xi_j^{n+1}\int\limits_{\Omega^{n+1}}U_j^{n+1}\xi_j^{n+1}\frac{\partial\xi_i^{n+1}}{\partial X^{n+1}}d\Omega$$
$$-\eta_j^{n+1}\int\limits_{\Omega^{n+1}}\frac{\partial\xi_i^{n+1}}{\partial X^{n+1}}d\Omega-\frac{1}{Re}\int\limits_{\Omega^{n+1}}\frac{\partial\xi_j^{n+1}}{\partial X^{n+1}}\frac{\partial\xi_i^{n+1}}{\partial X^{n+1}}d\Omega+\int\limits_{\Omega^{n+1}}\frac{\partial\xi_j^{n+1}}{\partial Y^{n+1}}\frac{\partial\xi_i^{n+1}}{\partial Y^{n+1}}d\Omega$$
$$+Gr_v\int\limits_{\Omega^{n+1}}U_j^{n+1}\xi_j^{n+1}\xi_i^{n+1}d\Omega+Gr_i\int\limits_{\Omega^{n+1}}\Big(U_j^{2n+2}\xi_j^{2n+2}+V_j^{2n+2}\xi_j^{2n+2}\Big)\xi_i^{n+1}d\Omega$$
$$=\frac{1}{Re}\oint\limits_{\Gamma}\xi_i^{n+1}\Big(n_x\frac{\partial\xi_j^{n+1}}{\partial X^{n+1}}\Big)d\Gamma+\frac{1}{Re}\oint\limits_{\Gamma}\xi_i^{n+1}\Big(n_y\frac{\partial\xi_j^{n+1}}{\partial Y^{n+1}}\Big)d\Gamma.$$

(4.44)

$$\frac{1}{\delta t}\int_{\Omega^n}\left(\sum_{j=1}^{m}V_j\xi_j\right)^{n+1}\left(\sum_{i=1}^{m}\tilde{V}_i\xi_i\right)d\Omega-\frac{1}{\delta t}\left(\left(\sum_{j=1}^{m}V_j\xi_j\right)^{n}\circ X^n\right)\left(\sum_{i=1}^{m}\tilde{V}_i\xi_i\right)d\Omega$$
$$+\sum_{i=1}^{l}q_i\eta_i\int_{\Omega^n}\left(\sum_{j=1}^{m}V_j\xi_j\right)\frac{\partial}{\partial Y}\left(\sum_{i=1}^{m}\tilde{V}_i\xi_i\right)d\Omega=\sum_{j=1}^{l}P_j\eta_j\int_{\Omega^n}\frac{\partial}{\partial Y}\left(\sum_{i=1}^{m}\tilde{V}_i\xi_i\right)d\Omega-$$
$$\frac{1}{Re}\int_{\Omega^n}\frac{\partial}{\partial X}\left(\sum_{j=1}^{m}V_j\xi_j\right)\frac{\partial}{\partial X}\left(\sum_{i=1}^{m}\tilde{V}_i\xi_i\right)d\Omega+\frac{1}{Re}\oint_{\Gamma}\left(\sum_{i=1}^{m}\tilde{V}_i\xi_i\right)\left(n_x\frac{\partial}{\partial X}\left(\sum_{j=1}^{m}V_j\xi_j\right)\right)d\Gamma$$
$$-\frac{1}{Re}\int_{\Omega^n}\frac{\partial}{\partial Y}\sum_{j=1}^{m}V_j\xi_j\frac{\partial}{\partial Y}\left(\sum_{i=1}^{m}\tilde{V}_i\xi_i\right)d\Omega+\frac{1}{Re}\oint_{\Gamma}\left(\sum_{i=1}^{m}\tilde{V}_i\xi_i\right)\left(n_y\frac{\partial}{\partial Y}\left(\sum_{j=1}^{m}V_j\xi_j\right)\right)d\Gamma$$
$$-Gr_v\int_{\Omega^n}\left(\sum_{j=1}^{m}V_j\xi_j\right)\left(\sum_{i=1}^{m}\tilde{V}_i\xi_i\right)d\Omega+Gr_i\int_{\Omega^n}\left[\left(\sum_{j=1}^{m}V_j\xi_j\right)^{2n+2}\right.$$
$$\left.+\left(\sum_{j=1}^{m}V_j\xi_j\right)^{2n+2}\left(\sum_{i=1}^{m}\tilde{V}_i\xi_i\right)d\Omega\right. \tag{4.45}$$

By Galerkin's approximation

$$\tilde{V}_h=\sum_{i=1}^{m}\tilde{V}i\xi_i.$$

(4.45) implies

$$\frac{1}{\delta t}\int\limits_{\Omega^n}\left(\sum_{j=1}^{m}V_j\xi_j\right)^{n+1}\sum_{i=1}^{m}\xi_i d\Omega-\frac{1}{\delta t}\left(\left(\sum_{j=1}^{m}V_j\xi_j\right)^{n}o\ X^n\right)\sum_{i=1}^{m}\xi_i d\Omega$$
$$+\sum_{i=1}^{l}q_i\eta_j\int\limits_{\Omega^n}\sum_{j=1}^{m}V_j\xi_j\frac{\partial}{\partial Y}\sum_{i=1}^{m}\xi_i d\Omega=\sum_{j=1}^{l}P_j\eta_j\int\limits_{\Omega^n}\frac{\partial}{\partial Y}\sum_{i=1}^{m}\xi_i d\Omega$$
$$-\frac{1}{Re}\int\limits_{\Omega^n}\frac{\partial}{\partial X}\sum_{j=1}^{m}V_j\xi_j\frac{\partial}{\partial X}\sum_{i=1}^{m}\xi_i d\Omega+\frac{1}{Re}\oint\limits_{\Gamma}\sum_{i=1}^{m}\xi_i\left(n_x\frac{\partial}{\partial X}\sum_{j=1}^{m}V_j\xi_j\right)d\Gamma$$
$$-\frac{1}{Re}\int\limits_{\Omega^n}\frac{\partial}{\partial Y}\sum_{j=1}^{m}V_j\xi_j\frac{\partial}{\partial Y}\sum_{i=1}^{m}\xi_i d\Omega+\frac{1}{Re}\oint\limits_{\Gamma}\sum_{i=1}^{m}\xi_i\left(n_y\frac{\partial}{\partial Y}\sum_{j=1}^{m}V_j\xi_j\right)d\Gamma$$
$$-Gr_v\int\limits_{\Omega^n}\sum_{j=1}^{m}V_j\xi_j\sum_{i=1}^{m}\tilde{V}_i\xi_i d\Omega-Gr_i\int\limits_{\Omega^n}\left(\left(\sum_{j=1}^{m}V_j\xi_j\right)^{2n+2}\right.$$
$$\left.+\left(\sum_{j=1}^{m}V_j\xi_j\right)^{2n+2}\right)\sum_{i=1}^{m}\tilde{V}_i\xi_i d\Omega.$$

$$\frac{1}{\delta t}\int\limits_{\Omega^n}\Big(\sum_{j=1}^{m}V_j\xi_j\Big)^{n+1}\sum_{i=1}^{m}\xi_i d\Omega-\frac{1}{\delta t}\Big(\Big(\sum_{j=1}^{m}V_j\xi_j\Big)^{n}o\ X^n\Big)\sum_{i=1}^{m}\xi_i d\Omega$$
$$+\sum_{i=1}^{l}q_i\eta_j\int\limits_{\Omega^n}\sum_{j=1}^{m}V_j\xi_j\sum_{i=1}^{m}\frac{\partial\xi_i}{\partial Y}d\Omega=\sum_{j=1}^{l}P_j\eta_j\int\limits_{\Omega^n}\sum_{i=1}^{m}\frac{\partial\xi_i}{\partial Y}d\Omega$$
$$-\frac{1}{Re}\int\limits_{\Omega^n}\sum_{j=1}^{m}\frac{\partial\xi_j}{\partial X}V_j\sum_{i=1}^{m}\frac{\partial\xi_i}{\partial X}d\Omega+\frac{1}{Re}\oint\limits_{\Gamma}\sum_{i=1}^{m}\xi_i\Big(n_x\sum_{j=1}^{m}\frac{\partial\xi_j}{\partial X}V_j\Big)d\Gamma$$
$$-\frac{1}{Re}\int\limits_{\Omega^n}\sum_{j=1}^{m}\frac{\partial\xi_j}{\partial Y}V_j\sum_{i=1}^{m}\frac{\partial\xi_i}{\partial Y}d\Omega+\frac{1}{Re}\oint\limits_{\Gamma}\sum_{i=1}^{m}\xi_i\Big(n_y\sum_{j=1}^{m}\frac{\partial\xi_j}{\partial Y}V_j\Big)d\Gamma$$
$$-Gr_v\int\limits_{\Omega^n}\sum_{j=1}^{m}V_j\xi_j\sum_{i=1}^{m}\xi_i d\Omega-Gr_i\int\limits_{\Omega^n}\Big(\Big(\sum_{j=1}^{m}V_j\xi_j\Big)^{2n+2}$$
$$+\Big(\sum_{j=1}^{m}V_j\xi_j\Big)^{2n+2}\Big)\sum_{i=1}^{m}\xi_i d\Omega.$$

$\Longrightarrow$

$$\frac{1}{\delta t}\int\limits_{\Omega^n}\Big(V_j\xi_j\Big)^{n+1}\xi_i d\Omega-\frac{1}{\delta t}\Big(\Big(V_j\xi_j\Big)^{n}o\ X^n\Big)\xi_i d\Omega+\eta_j\int\limits_{\Omega^n}V_j\xi_j\frac{\partial\xi_i}{\partial Y}d\Omega$$
$$=\eta_j\int\limits_{\Omega^n}\frac{\partial\xi_i}{\partial Y}d\Omega-\frac{1}{Re}\int\limits_{\Omega^n}\frac{\partial\xi_j}{\partial X}\frac{\partial\xi_i}{\partial X}d\Omega+\frac{1}{Re}\oint\limits_{\Gamma}\xi_i\Big(n_x\frac{\partial\xi_j}{\partial X}\Big)d\Gamma$$
$$-\frac{1}{Re}\int\limits_{\Omega^n}\frac{\partial\xi_j}{\partial Y}\frac{\partial\xi_i}{\partial Y}d\Omega+\frac{1}{Re}\oint\limits_{\Gamma}\xi_i\Big(n_y\frac{\partial\xi_j}{\partial Y}\Big)d\Gamma-Gr_v\int\limits_{\Omega^n}V_j\xi_j\xi_i d\Omega$$
$$-Gr_i\int\limits_{\Omega^n}\Big(\Big(V_j\xi_j\Big)^{2n+2}+\Big(V_j\xi_j\Big)^{2n+2}\Big)\xi_i d\Omega.$$

$\Longrightarrow$

$$\frac{1}{\delta t}\int\limits_{\Omega^{n+1}}V_j^{n+1}\xi_j^{n+1}\xi_i^{n+1}d\Omega-\frac{1}{\delta t}\Big(V_j^n\xi_j^n o\ X^n\Big)\xi_i^{n+1}d\Omega+\eta_j^{n+1}\int\limits_{\Omega^{n+1}}V_j^{n+1}\xi_j^{n+1}\frac{\partial\xi_i^{n+1}}{\partial Y^{n+1}}d\Omega$$
$$=\eta_j^{n+1}\int\limits_{\Omega^{n+1}}\frac{\partial\xi_i^{n+1}}{\partial Y^{n+1}}d\Omega-\frac{1}{Re}\int\limits_{\Omega^{n+1}}\frac{\partial\xi_j^{n+1}}{\partial X^{n+1}}\frac{\partial\xi_i^{n+1}}{\partial X^{n+1}}d\Omega+\frac{1}{Re}\oint\limits_{\Gamma}\xi_i^{n+1}\Big(n_x\frac{\partial\xi_j^{n+1}}{\partial X^{n+1}}\Big)d\Gamma$$
$$-\frac{1}{Re}\int\limits_{\Omega^{n+1}}\frac{\partial\xi_j^{n+1}}{\partial Y^{n+1}}\frac{\partial\xi_i^{n+1}}{\partial Y^{n+1}}d\Omega+\frac{1}{Re}\oint\limits_{\Gamma}\xi_i^{n+1}\Big(n_y\frac{\partial\xi_j^{n+1}}{\partial Y^{n+1}}\Big)d\Gamma$$
$$-Gr_v\int\limits_{\Omega^{n+1}}V_j^{n+1}\xi_j^{n+1}\xi_i^{n+1}d\Omega-Gr_i\int\limits_{\Omega^{n+1}}\Big(V_j^{2n+2}\xi_j^{2n+2}+V_j^{2n+2}\xi_j^{2n+2}\Big)\xi_i^{n+1}d\Omega \tag{4.46}$$

(4.42) $\Longrightarrow$

$$\frac{1}{\delta t}\int\limits_{\Omega^n}\left(\sum_{j=1}^{m}T_j\xi_j\right)^{n+1}\sum_{i=1}^{m}\tilde{T}i\xi_i d\Omega-\frac{1}{\delta t}\left(\left(\sum_{j=1}^{m}T_j\xi_j\right)^{n}\ o\ X^n\right)\sum_{i=1}^{m}\tilde{T}i\xi_i d\Omega$$

$$=-\frac{1}{RePr}\int\limits_{\Omega^n}\frac{\partial}{\partial X}\sum_{j=1}^{m}T_j\xi_j\frac{\partial}{\partial X}\sum_{i=1}^{m}\tilde{T}i\xi_i d\Omega+\frac{1}{RePr}\oint\limits_{\Gamma}\sum_{i=1}^{m}\tilde{T}i\xi_i\left(n_x\frac{\partial}{\partial X}\sum_{j=1}^{m}T_j\xi_j\right)d\Gamma$$

$$-\frac{1}{RePr}\int\limits_{\Omega^n}\frac{\partial}{\partial Y}\sum_{j=1}^{m}T_j\xi_j\frac{\partial}{\partial Y}\sum_{i=1}^{m}\tilde{T}i\xi_i d\Omega+\frac{1}{RePr}\oint\limits_{\Gamma}\sum_{i=1}^{m}\tilde{T}i\xi_i\left(n_y\frac{\partial}{\partial Y}\sum_{j=1}^{m}T_j\xi_j\right)d\Gamma$$

$$-\frac{Rd}{RePr}\int\limits_{\Omega^n}\frac{\partial}{\partial Y}\sum_{j=1}^{m}T_j\xi_j\frac{\partial}{\partial Y}\sum_{i=1}^{m}\tilde{T}i\xi_i d\Omega+\frac{Rd}{RePr}\oint\limits_{\Gamma}\sum_{i=1}^{m}\tilde{T}i\xi_i\left(n_y\frac{\partial}{\partial Y}\sum_{j=1}^{m}T_j\xi_j\right)d\Gamma \tag{4.47}$$

By Galerkins approximation

$$\tilde{T}_h=\sum_{i=1}^{m}\tilde{T}i\xi_i$$

(4.47) $\Longrightarrow$

$$\frac{1}{\delta t}\int\limits_{\Omega^n}\left(\sum_{j=1}^{m}T_j\xi_j\right)^{n+1}\sum_{i=1}^{m}\xi_i d\Omega-\frac{1}{\delta t}\left(\left(\sum_{j=1}^{m}T_j\xi_j\right)^{n}\ o\ X^n\right)\sum_{i=1}^{m}\xi_i d\Omega$$

$$=-\frac{1}{RePr}\int\limits_{\Omega^n}\frac{\partial}{\partial X}\sum_{j=1}^{m}T_j\xi_j\frac{\partial}{\partial X}\sum_{i=1}^{m}\xi_i d\Omega+\frac{1}{RePr}\oint\limits_{\Gamma}\sum_{i=1}^{m}\xi_i\left(n_x\frac{\partial}{\partial X}\sum_{j=1}^{m}T_j\xi_j\right)d\Gamma$$

$$-\frac{1}{RePr}\int\limits_{\Omega^n}\frac{\partial}{\partial Y}\sum_{j=1}^{m}T_j\xi_j\frac{\partial}{\partial Y}\sum_{i=1}^{m}\xi_i d\Omega+\frac{1}{RePr}\oint\limits_{\Gamma}\sum_{i=1}^{m}\xi_i\left(n_y\frac{\partial}{\partial Y}\sum_{j=1}^{m}T_j\xi_j\right)d\Gamma$$

$$-\frac{Rd}{RePr}\int\limits_{\Omega^n}\frac{\partial}{\partial Y}\sum_{j=1}^{m}T_j\xi_j\frac{\partial}{\partial Y}\sum_{i=1}^{m}\xi_i d\Omega+\frac{Rd}{RePr}\oint\limits_{\Gamma}\sum_{i=1}^{m}\xi_i\left(n_y\frac{\partial}{\partial Y}\sum_{j=1}^{m}T_j\xi_j\right)d\Gamma.$$

$$\frac{1}{\delta t}\int\limits_{\Omega^n}\left(\sum_{j=1}^{m}T_j\xi_j\right)^{n+1}\sum_{i=1}^{m}\xi_i d\Omega-\frac{1}{\delta t}\left(\left(\sum_{j=1}^{m}T_j\xi_j\right)^{n}\ o\ X^n\right)\sum_{i=1}^{m}\xi_i d\Omega$$
$$=-\frac{1}{RePr}\int\limits_{\Omega^n}\sum_{j=1}^{m}\frac{\partial\xi_j}{\partial X}T_j\sum_{i=1}^{m}\frac{\partial\xi_i}{\partial X}d\Omega+\frac{1}{RePr}\oint\limits_{\Gamma}\sum_{i=1}^{m}\xi_i\left(n_x\sum_{j=1}^{m}\frac{\partial\xi_j}{\partial X}T_j\right)d\Gamma$$
$$-\frac{1}{RePr}\int\limits_{\Omega^n}\sum_{j=1}^{m}\frac{\partial\xi_j}{\partial Y}T_j\sum_{i=1}^{m}\frac{\partial\xi_i}{\partial Y}d\Omega+\frac{1}{Re}\frac{1}{Pr}\oint\limits_{\Gamma}\sum_{i=1}^{m}\xi_i\left(n_y\sum_{j=1}^{m}\frac{\partial\xi_j}{\partial Y}T_j\right)d\Gamma$$
$$-\frac{Rd}{RePr}\int\limits_{\Omega^n}\sum_{j=1}^{m}\frac{\partial\xi_j}{\partial Y}T_j\sum_{i=1}^{m}\frac{\partial\xi_i}{\partial Y}d\Omega+\frac{Rd}{RePr}\oint\limits_{\Gamma}\sum_{i=1}^{m}\xi_i\left(n_y\sum_{j=1}^{m}\frac{\partial\xi_j}{\partial Y}T_j\right)d\Gamma.$$

$\Longrightarrow$

$$\frac{1}{\delta t}\int\limits_{\Omega^n}\left(T_j\xi_j\right)^{n+1}\xi_i d\Omega-\frac{1}{\delta t}\left(\left(T_j\xi_j\right)^{n}\ o\ X^n\right)\xi_i d\Omega=-\frac{1}{RePr}\int\limits_{\Omega^n}\frac{\partial\xi_j}{\partial X}\frac{\partial\xi_i}{\partial X}d\Omega$$
$$+\frac{1}{RePr}\oint\limits_{\Gamma}\xi_i\left(n_x\frac{\partial\xi_j}{\partial X}\right)d\Gamma-\frac{1}{RePr}\int\limits_{\Omega^n}\frac{\partial\xi_j}{\partial Y}\frac{\partial\xi_i}{\partial Y}d\Omega+\frac{1}{RePr}\oint\limits_{\Gamma}\xi_i\left(n_y\frac{\partial\xi_j}{\partial Y}\right)d\Gamma$$
$$-\frac{Rd}{RePr}\int\limits_{\Omega^n}\frac{\partial\xi_j}{\partial Y}\frac{\partial\xi_i}{\partial Y}d\Omega+\frac{Rd}{Re}\frac{1}{Pr}\oint\limits_{\Gamma}\xi_i\left(n_y\frac{\partial\xi_j}{\partial Y}\right)d\Gamma.$$

$\Longrightarrow$

$$\frac{1}{\delta t}\int\limits_{\Omega^{n+1}}T_j^{n+1}\xi_j^{n+1}\xi_i^{n+1}d\Omega-\frac{1}{\delta t}\left(T_j^n\xi_j^n\ o\ X^n\right)\xi_i^{n+1}d\Omega$$
$$=-\frac{1}{RePr}\int\limits_{\Omega^{n+1}}\frac{\partial\xi_j^{n+1}}{\partial X^{n+1}}\frac{\partial\xi_i^{n+1}}{\partial X^{n+1}}d\Omega+\frac{1}{RePr}$$
$$\oint\limits_{\Gamma}\xi_i^{n+1}\left(n_x\frac{\partial\xi_j^{n+1}}{\partial X^{n+1}}\right)d\Gamma-\frac{1}{RePr}\int\limits_{\Omega^{n+1}}\frac{\partial\xi_j^{n+1}}{\partial Y^{n+1}}\frac{\partial\xi_i^{n+1}}{\partial Y^{n+1}}d\Omega \tag{4.48}$$
$$+\frac{1}{RePr}\oint\limits_{\Gamma}\xi_i^{n+1}\left(n_y\frac{\partial\xi_j^{n+1}}{\partial Y^{n+1}}\right)d\Gamma-\frac{Rd}{RePr}\int\limits_{\Omega^{n+1}}\frac{\partial\xi_j^{n+1}}{\partial Y^{n+1}}\frac{\partial\xi_i^{n+1}}{\partial Y^{n+1}}d\Omega$$
$$+\frac{Rd}{RePr}\oint\limits_{\Gamma}\xi_i^{n+1}\left(n_y\frac{\partial\xi_j^{n+1}}{\partial Y^{n+1}}\right)d\Gamma.$$

From Eqs. (4.44), (4.46) and (4.48), we get the discretized system of nonlinear algebraic equations as

$$[A^*(u,v)]\{X^*\}=\{F^*\}+\{Q^*\}.$$

The matrix notation of $A^*(u,v),\ X^*,\ F^*$ and Q^* can be written as

$$\underbrace{\begin{bmatrix} S^{11} & S^{12} & B_1 & S^{14} \\ S^{21} & S^{22} & B_2 & S^{24} \\ B_1^T & B_2^T & S^{33} & S^{34} \\ S^{41} & S^{42} & S^{43} & S^{44} \end{bmatrix}}_{A^*} \underbrace{\begin{bmatrix} U \\ V \\ P \\ T \end{bmatrix}}_{X^*} = \underbrace{\begin{bmatrix} F_1 \\ F_2 \\ F_3 \\ F_4 \end{bmatrix}}_{F^*} + \underbrace{\begin{bmatrix} Q_1 \\ Q_2 \\ Q_3 \\ Q_4 \end{bmatrix}}_{Q^*}. \tag{4.49}$$

Here A^*, X^*, F^* and Q^* are called block stiffness matrix, block solution vector, block load vector and block boundary vector respectively.

The local elemental entries of block stiffness matrix are given as

$$\begin{aligned} S^{11} = & \frac{1}{\delta t} \int\limits_{\Omega^{n+1}} U_j^{n+1} \xi_j^{n+1} \xi^{n+1} i d\Omega - \frac{1}{\delta t} \Big(U j^n \xi_j^n o\ X^n \Big) \xi_i^{n+1} d\Omega \\ & + \xi_j^{n+1} \int\limits_{\Omega^{n+1}} U_j^{n+1} \xi_j^{n+1} \frac{\partial \xi_i^{n+1}}{\partial X^{n+1}} d\Omega + \frac{1}{Re} \int\limits_{\Omega^{n+1}} \frac{\partial \xi_j^{n+1}}{\partial X^{n+1}} \frac{\partial \xi_i^{n+1}}{\partial X^{n+1}} d\Omega \\ & + \frac{1}{Re} \int\limits_{\Omega^{n+1}} \frac{\partial \xi_j^{n+1}}{\partial Y^{n+1}} \frac{\partial \xi_i^{n+1}}{\partial Y^{n+1}} d\Omega + Gr_v \int\limits_{\Omega^{n+1}} U_j^{n+1} \xi_j^{n+1} \xi_i^{n+1} d\Omega \\ & + Gr_i \int\limits_{\Omega^{n+1}} \Big(U_j^{2n+2} \xi_j^{2n+2} + V_j^{2n+2} \xi_j^{2n+2} \Big) \xi_i^{n+1} d\Omega, \end{aligned}$$

$$S^{12} = Gr_i \int\limits_{\Omega^{n+1}} \Big(U_j^{2n+2} \xi_j^{2n+2} + V_j^{2n+2} \xi_j^{2n+2} \Big) \xi_i^{n+1} d\Omega,$$

$$S^{14} = 0,$$

$$S^{21} = -Gr_i \int\limits_{\Omega^{n+1}} \Big(V_j^{2n+2} \xi_j^{2n+2} + U_j^{2n+2} \xi_j^{2n+2} \Big) \xi_i^{n+1} d\Omega,$$

$$S^{22} = \frac{1}{\delta t}\int\limits_{\Omega^{n+1}} V_j^{n+1}\xi_j^{n+1}\xi_i^{n+1}d\Omega - \frac{1}{\delta t}\Big(V_j^n\xi_j^n o\ X^n\Big)\xi_i^{n+1}d\Omega$$
$$+\eta_j^{n+1}\int\limits_{\Omega^{n+1}} V_j^{n+1}\xi_j^{n+1}\frac{\partial\xi_i^{n+1}}{\partial Y^{n+1}}d\Omega + \frac{1}{Re}\int\limits_{\Omega^{n+1}}\frac{\partial\xi_j^{n+1}}{\partial X^{n+1}}\frac{\partial\xi_i^{n+1}}{\partial X^{n+1}}d\Omega\Big)$$
$$+\frac{1}{Re}\int\limits_{\Omega^{n+1}}\frac{\partial\xi_j^{n+1}}{\partial Y^{n+1}}\frac{\partial\xi_i^{n+1}}{\partial Y^{n+1}}d\Omega - Gr_v\int\limits_{\Omega^{n+1}} V_j^{n+1}\xi_j^{n+1}\xi_i^{n+1}d\Omega$$
$$-Gr_i\int\limits_{\Omega^{n+1}}\Big(V_j^{2n+2}\xi_j^{2n+2} + V_j^{2n+2}\xi_j^{2n+2}\Big)\xi_i^{n+1}d\Omega,$$

$$S^{24}=0,\qquad S^{33}=0,\qquad S^{34}=0,\qquad S^{41}=0,\qquad S^{42}=0,\qquad S^{43}=0$$

$$S^{44} = \frac{1}{\delta t}\int\limits_{\Omega^{n+1}} T_j^{n+1}\xi_j^{n+1}\xi_i^{n+1}d\Omega - \frac{1}{\delta t}\Big(T_j^n\xi_j^n\ o\ X^n\Big)\xi_i^{n+1}d\Omega$$
$$+\frac{1}{RePr}\int\limits_{\Omega^{n+1}}\frac{\partial\xi_j^{n+1}}{\partial X^{n+1}}\frac{\partial\xi_i^{n+1}}{\partial X^{n+1}}d\Omega + \frac{1}{RePr}\int\limits_{\Omega^{n+1}}\frac{\partial\xi_j^{n+1}}{\partial Y^{n+1}}\frac{\partial\xi_i^{n+1}}{\partial Y^{n+1}}d\Omega$$
$$+\frac{Rd}{RePr}\int\limits_{\Omega^{n+1}}\frac{\partial\xi_j^{n+1}}{\partial Y^{n+1}}\frac{\partial\xi_i^{n+1}}{\partial Y^{n+1}}d\Omega - \frac{Rd}{RePr}\oint\limits_{\Gamma}\xi_i^{n+1}\Big(n_y\frac{\partial\xi_j^{n+1}}{\partial Y^{n+1}}\Big)d\Gamma.$$

The entries $S^{13},\ S^{23}$ and $S^{31},\ S^{32}$ are the pressure matrices with their respective transposes can be written as

$$B_1^{ij} = \sum_{j=1}^{l}\int\limits_{\Omega^{n+1}}\frac{\partial\xi_i}{\partial x^{n+1}}\eta_j^{n+1}d\Omega\{P_j^{n+1}\},$$

$$B_2^{ij} = \sum_{j=1}^{l}\int\limits_{\Omega^{n+1}}\frac{\partial\xi_i}{\partial y^{n+1}}\eta_j^{n+1}d\Omega\{P_j^{n+1}\},$$

$$(B_1^{ij})^t = \sum_{j=1}^{l}\int\limits_{\Omega^{n+1}}\frac{\partial\eta_j^{n+1}}{\partial x^{n+1}}\xi_i d\Omega\{P_j^{n+1}\},$$

$$(B_2^{ij})^t = \sum_{j=1}^{l} \int_{\Omega^{n+1}} \frac{\partial \eta_j^{n+1}}{\partial y^{n+1}} \xi_i d\Omega \{P_j^{n+1}\},$$

$$F_1 = 0, \qquad F_2 = 0, \qquad F_3 = 0, \qquad F_4 = 0,$$

$$Q_3 = 0, \tag{4.50}$$

$$Q_1 = \sum_{j=1}^{m} \oint_{\Gamma} \xi_i \left[\left(n_x \frac{\partial \xi_j^{n+1}}{\partial x^{n+1}} \right) + \left(n_y \frac{\partial \xi_j^{n+1}}{\partial y^{n+1}} \right) \right] d\Gamma \{U_j^{n+1}\},$$

$$Q_2 = \sum_{j=1}^{m} \oint_{\Gamma} \xi_i \left[\left(n_x \frac{\partial \xi_j^{n+1}}{\partial x^{n+1}} \right) + \left(n_y \frac{\partial \xi_j^{n+1}}{\partial y^{n+1}} \right) \right] d\Gamma \{V_j^{n+1}\},$$

$$Q_4 = \sum_{j=1}^{m} \oint_{\Gamma} \xi_i \left[\left(n_x \frac{\partial \xi_j^{n+1}}{\partial x^{n+1}} \right) + \left(n_y \frac{\partial \xi_j^{n+1}}{\partial y^{n+1}} \right) \right] d\Gamma \{T_j^{n+1}\}.$$

The discrete system of non-linear algebraic equations in matrix form can be written as:

$$\begin{bmatrix} S^{11} & S^{12} & B_1 & 0 \\ S^{21} & S^{22} & B_2 & 0 \\ B_1^T & B_2^T & 0 & 0 \\ 0 & 0 & 0 & S^{44} \end{bmatrix} \begin{bmatrix} U \\ V \\ P \\ T \end{bmatrix} = \begin{bmatrix} 0 \\ 0 \\ 0 \\ 0 \end{bmatrix} + \begin{bmatrix} Q_1 \\ Q_2 \\ 0 \\ Q_4 \end{bmatrix}. \tag{4.51}$$

(4.51) is solved through FEM code Free Fem++. This system along with the geometry and boundary conditions are implemented in Free Fem++. The code is used to compute the solution for variant parameter on the computational domain (see Figure 4.1).

4.6 Results and Discussion

This section is devoted to present the numerical results computed Results through the finite element method for the presented model problem in the previous section. Before analyzing the Darcy–Forchheimer radiative flow in a lid-driven cavity, it is essential to validate the accuracy of the numerical code implemented in FreeFEM++.

For this purpose, we consider the classical lid-driven cavity problem without porous medium effects, without thermal transport, and without radiation. This configuration has been extensively studied in the literature, and benchmark results provided by Ghia et al. [31] are used for validation.

The computational setup for validation uses the same geometry as our main problem: a unit square cavity with a moving top lid. The Reynolds numbers considered are $Re = 100$, 400, and 1000, matching the reference benchmark. The top wall moves with a uniform velocity $U = 1$, and the other three walls are stationary with no-slip boundary conditions.

Tables 4.1 and 4.2 present a comparison between the Present Results from our `FreeFEM++` simulations and the benchmark results of Ghia et al. [31].

The comparisons are carried out along the vertical centerline at $X = 0.5$ for the horizontal velocity component U and along the horizontal centerline at $Y = 0.5$ for the vertical velocity component V.

From Tables 4.1 and 4.2, it can be observed that the Present Results are in good agreement with the benchmark data [31].

The comparison with the benchmark data demonstrates that the present numerical model accurately captures the primary flow characteristics in a classical lid-driven cavity.

Therefore, the same numerical framework can be confidently applied to analyze the combined effects of Re, Gr_v, Gr_i, Pr, and Rd on the velocity and temperature fields in the porous cavity.

TABLE 4.1: Validation: U-velocity along the vertical centreline ($X = 0.5$). Reference values from Ghia et al. [31].

Y	Re = 100		Re = 400		Re = 1000	
	Ghia	Present Results	Ghia	Present Results	Ghia	Present Results
0.9766	0.84123	0.84051237	0.75837	0.75682311	0.65928	0.65693245
0.7344	0.00332	0.00345127	0.16256	0.16421134	0.18719	0.18914821
0.6172	-0.13641	-0.13521744	0.02135	0.02189563	0.05702	0.05800277
0.5000	-0.20581	-0.20403766	-0.11477	-0.11602854	-0.06080	-0.06154789
0.2813	-0.15662	-0.15788214	-0.32726	-0.32991347	-0.27805	-0.28132154
0.1016	-0.06434	-0.06511255	-0.14612	-0.14783712	-0.29730	-0.30104893

TABLE 4.2: Validation: V-velocity along the horizontal centreline ($Y = 0.5$). Reference values from Ghia et al. [31].

X	Re = 100		Re = 400		Re = 1000	
	Ghia	Present Results	Ghia	Present Results	Ghia	Present Results
0.0703	0.10091	0.10168251	0.19713	0.19854319	0.29012	0.29387993
0.2344	0.17527	0.17408364	0.30174	0.30422111	0.32235	0.32605872
0.5000	0.05454	0.05400371	0.05186	0.05262789	0.02526	0.02583744
0.8047	-0.24533	-0.24381126	-0.38598	-0.38221793	-0.31966	-0.31787914
0.9063	-0.16914	-0.17084311	-0.23827	-0.24067219	-0.51500	-0.52089472
0.9688	-0.05906	-0.05950812	-0.12146	-0.12293428	-0.21388	-0.21708644

TABLE 4.3: Effects of radiation on temperature when $P_r = 1,\ R_e = 50,\ R_d = 0.1,\ \mathrm{Gr}_i = 0.5,\ \mathrm{Gr}_v = 0.5$

Rd	$T(0.5,\ 0.25)$	$T(0.5,\ 0.5)$
0.02	0.372711	0.0737924
0.5	0.214288	0.013398
0.7	0.110104	0.0016436
0.8	0.0510762	0.000147085

Table 4.3 presents the variation of the temperature distribution at two different locations within the cavity, namely $(0.5, 0.25)$ and $(0.5, 0.5)$, for different values of the radiation parameter Rd, while keeping $Pr = 1$, $Re = 50$, $Gr_i = 0.5$, and $Gr_v = 0.5$. It can be observed that as Rd increases, the temperature values at both points decrease significantly.

This indicates that stronger radiation effects enhance the rate of heat transfer from the fluid, thereby lowering the fluid temperature inside the cavity. For small values of Rd (e.g., 0.02), relatively higher temperatures are maintained at both points, while for larger values (e.g., 0.8), the temperatures are drastically reduced. This clearly demonstrates the cooling influence of radiation on the thermal field of the porous cavity flow.

TABLE 4.4: Effects of Grashof number Gr_i on temperature T and U-velocity when $\mathrm{P}_r = 1,\ R_e = 50,\ Rd = 0.02,\ \mathrm{Gr}_v = 0.5$

Gr_i	T(0.5, 0.25)	T(0.5, 0.5)	|U(0.5, 0.25)|	|U(0.5, 0.5)|
0.5	0.372711	0.0737924	0.0943992	0.157926
0.4	0.372667	0.0737625	0.0954542	0.158242
0.1	0.372520	0.0736639	0.0984794	0.159259
0.01	0.372471	0.0736316	0.0994199	0.159584
0.001	0.372466	0.0736283	0.0995145	0.159618

Table 4.4 shows the effect of the porosity parameter Gr_i on temperature and the horizontal U velocity at two fixed locations inside the cavity. The parameters are fixed as $Pr = 1$, $Re = 50$, $Rd = 0.02$, and $Gr_v = 0.5$. The results reveal that the temperature values at both positions remain nearly constant with varying Gr_i, suggesting that the porosity parameter Gr_i has a negligible effect on the thermal distribution. However, the velocity components $|U(0.5, 0.25)|$ and $|U(0.5, 0.5)|$ show sensitivity to Gr_i. As Gr_i decreases, the velocity magnitude increases slightly, implying that reduction in porous resistance allows stronger convective motion. This behavior highlights that Gr_i primarily influences the momentum transport rather than the thermal field.

TABLE 4.5: Effects of Grashof number Gr_v on temperature T and U-velocity when $P_r = 1$, $R_e = 50$, $R_d = 0.02$, $\mathrm{Gr}_i = 0.5$

Gr_v	$T(0.5, 0.25)$	$T(0.5, 0.5)$	$\lvert U(0.5, 0.25)\rvert$	$\lvert U(0.5, 0.5)\rvert$
0.5	0.372711	0.0737924	0.0943992	0.157926
0.4	0.371503	0.073049	0.094828	0.163312
0.1	0.367688	0.0704416	0.095601	0.182471
0.01	0.366491	0.0695999	0.0956234	0.189271
0.001	0.366370	0.0695139	0.0995629	0.189982

Table 4.5 examines the impact of another porosity-related parameter, Gr_v, on both temperature and horizontal U velocity. The governing parameters are kept at $Pr = 1$, $Re = 50$, $Rd = 0.02$, and $Gr_i = 0.5$.

The results indicate that as Gr_v decreases, the temperature at both positions reduces slightly, but more importantly, the velocity values increase. For instance, when Gr_v is lowered from 0.5 to 0.001, the velocity at $(0.5, 0.25)$ rises from approximately 0.1579 to 0.18998.

This trend signifies that decreasing Gr_v enhances the permeability of the porous medium, leading to less resistance against the fluid motion and hence stronger convective currents. Thus, Gr_v acts as a control parameter for regulating the convective strength within the porous cavity.

TABLE 4.6: Effects of Prandtl number Pr on temperature T at two different points when $\mathrm{R}_e = 500,\ R_d = 0.1,\ \mathrm{Gr}_i = 0.5,\ \mathrm{Gr}_v = 0.5$

Pr	$T(0.5,\ 0.25)$	$T(0.5,\ 0.5)$
0.001	0.750221	0.500432
0.11	0.33711	0.055555
0.23	0.166162	0.00583517
1	0.0040729	2.06849×10^{-8}
2	5.80684×10^{-5}	4.07439×10^{-13}
5	2.26131×10^{-9}	1.51074×10^{-18}

Table 4.6 highlights the influence of the Prandtl number Pr on the temperature at two distinct positions. For this case, the parameters are fixed as $Re = 500$, $Rd = 0.1$, $Gr_i = 0.5$, and $Gr_v = 0.5$. The results show a significant dependence of temperature on Pr. At small values of Pr (e.g., 0.001), the temperature at $(0.5, 0.25)$ and $(0.5, 0.5)$ is higher, while increasing Pr reduces the temperature drastically. This is consistent with the physical interpretation of Pr, which measures the relative importance of momentum diffusivity to thermal diffusivity. At higher Pr, heat diffuses more slowly, leading to reduced thermal penetration into the fluid domain. The rapid drop of temperature for large Pr values indicates stronger thermal boundary layer thinning.

TABLE 4.7: Effects of Grashof number Gr_i on temperature T and U-velocity when $\mathrm{P}_r = 0.001,\ R_e = 500,\ R_d = 0.1,\ \mathrm{Gr}_v = 0.5$

Gr_i	$T(0.5,\ 0.25)$	$T(0.5,\ 0.5)$	$\lvert U(0.5,\ 0.25)\rvert$	$\lvert U(0.5,\ 0.5)\rvert$
0.5	0.750221	0.500432	0.0297321	0.0438813
0.4	0.750223	0.500435	0.0300798	0.0442217
0.1	0.750227	0.500446	0.0311647	0.0452716
0.01	0.750229	0.500450	0.0315030	0.0455950
0.001	0.750231	0.500451	0.0394409	0.0457995

Table 4.7 extends the analysis of Gr_i to the case of $Pr = 0.001$, $Re = 500$, $Rd = 0.1$, and $Gr_v = 0.5$. The results confirm the earlier observation that Gr_i has little influence on the temperature field, with nearly identical values of $T(0.5, 0.25)$ and $T(0.5, 0.5)$ across all Gr_i. However, the velocity values show modest variation: as Gr_i decreases, both $|U(0.5, 0.25)|$ and $|U(0.5, 0.5)|$ increase.

This again suggests that the effect of porosity through Gr_i is more significant on momentum transport, with reduced resistance enhancing the strength of lid-driven convection.

TABLE 4.8: Effects of Grashof number Gr_v on temperature T and U-velocity when $\mathrm{P}_r = 0.001$, $R_e = 500$, $R_d = 0.1$, $\mathrm{Gr}_i = 0.5$

Gr_v	$T(0.5, 0.25)$	$T(0.5, 0.5)$	$\lvert U(0.5, 0.25)\rvert$	$\lvert U(0.5, 0.5)\rvert$
0.5	0.750221	0.500432	0.0297321	0.0438813
0.4	0.750213	0.500431	0.0294409	0.0451995
0.1	0.750185	0.500422	0.0278522	0.0500868
0.01	0.750175	0.500417	0.0270723	0.0518727
0.001	0.750174	0.500417	0.0269840	0.0520601

Finally, Table 4.8 demonstrates the influence of Gr_v on temperature and velocity for the case $Pr = 0.001$, $Re = 500$, $Rd = 0.1$, and $Gr_i = 0.5$. As observed earlier, the temperature field is relatively insensitive to Gr_v. However, the velocity field is strongly affected: decreasing Gr_v from 0.5 to 0.001 results in higher velocities, reflecting the enhanced convective motion due to reduced porous drag.

Figure 4.2 illustrates the U-velocity contours inside the porous square cavity for different Reynolds numbers (Re), while keeping other parameters fixed at $t = 1.5$, $Pr = 5.5$, $Rd = 1$, $Gr_i = 0.001$, and $Gr_v = 0.5$. At low $Re = 1$, the flow is in the creeping regime where viscous forces dominate, resulting in smooth and symmetric contours with a single weak recirculation cell.

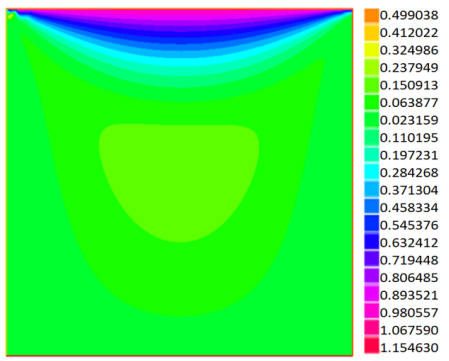

(a) $Re = 1$

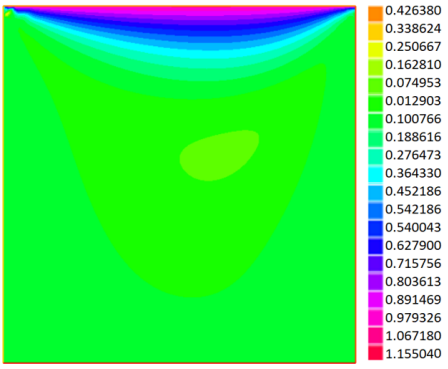

(b) $Re = 50$

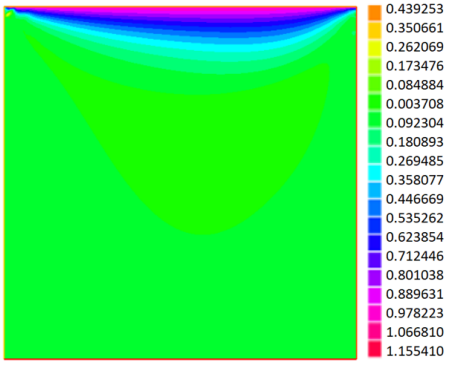

(c) $Re = 100$

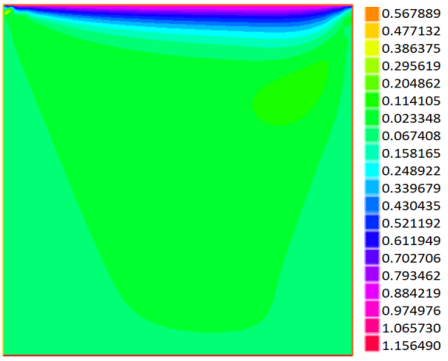

(d) $Re = 300$

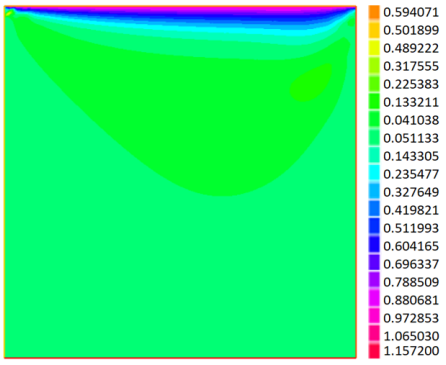

(e) $Re = 500$

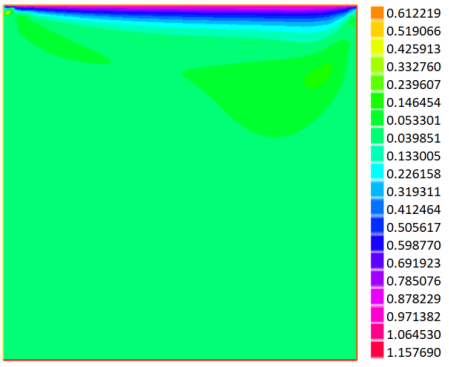

(f) $Re = 700$

FIGURE 4.2: U-velocity plots for varying values of Re. Other parameters are: $t = 1.5,\ Pr = 5.5,\ Rd = 1,\ Gr_i = 0.001,\ Gr_v = 0.5$.

As Re increases to 50 and 100, the influence of the moving lid becomes more pronounced, leading to stronger circulation and thinner boundary layers near the top wall.

The primary vortex at the cavity center becomes well-defined, and the flow

gradually transitions from viscous- to inertia-dominated behavior.

For $Re = 300$, the flow remains steady and laminar with a dominant single vortex, but velocity gradients intensify near the upper boundary.

At $Re = 500$, secondary vortices begin to form at the lower corners, indicating the onset of more complex flow structures.

Finally, at $Re = 700$, the primary vortex strengthens further, secondary vortices become more prominent, and a small tertiary vortex emerges near the top-left corner, marking a transition toward a multi-vortex regime driven by strong inertial effects.

Overall, increasing Re enhances momentum transport from the moving lid, sharpens boundary layers, and promotes the development of secondary and tertiary vortices, highlighting the progressive transition from viscous-dominated to inertia-driven cavity flow.

Figure 4.3 illustrates the V-velocity contours inside the porous cavity for different Reynolds numbers (Re), while keeping the other governing parameters fixed at $t = 1.5$, $Pr = 5.5$, $Rd = 1$, $Gr_i = 0.0001$, and $Gr_v = 0.5$.

These contours provide a clear depiction of the flow recirculation patterns and convective strength within the cavity under varying inertial effects. Subfigures (a)–(f) correspond to $Re = 1$, 100, 200, 700, 1000, and 1500, respectively.

At a very low Reynolds number ($Re = 1$), viscous forces dominate the flow, resulting in a highly diffusive velocity field. A strong recirculating cell forms in the central region of the cavity, occupying a significant portion of the domain.

The contours exhibit smooth gradients, and the magnitude of the V-velocity remains relatively high, consistent with the characteristics of creeping flow where viscous diffusion primarily governs momentum transport.

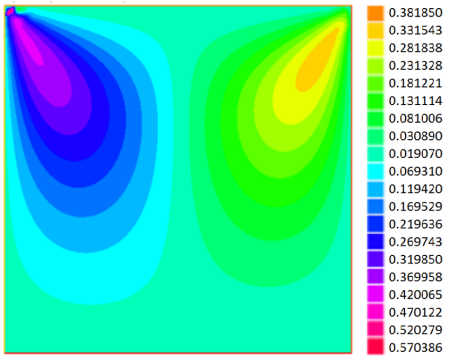

(a) $Re = 1$

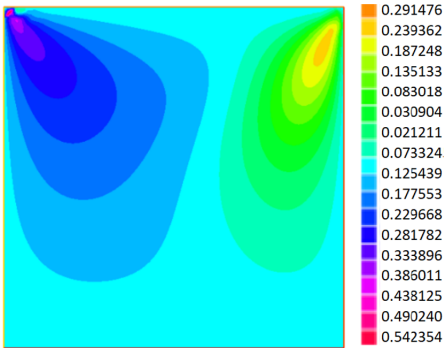

(b) $Re = 100$

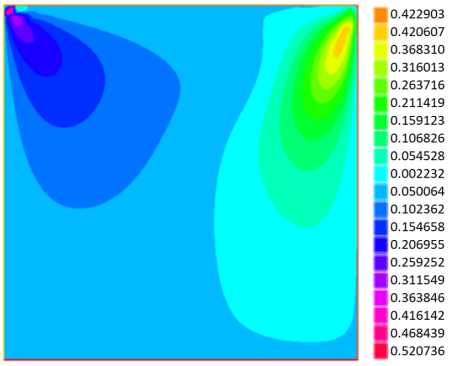

(c) $Re = 200$

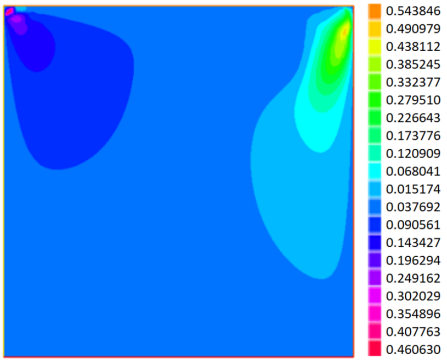

(d) $Re = 700$

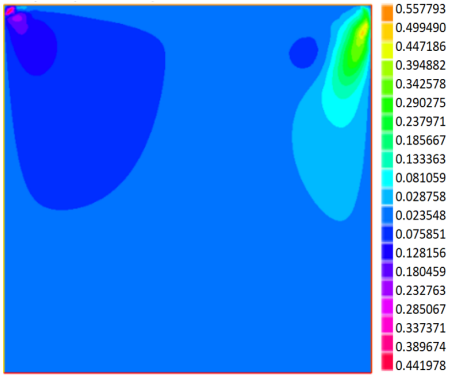

(e) $Re = 1000$

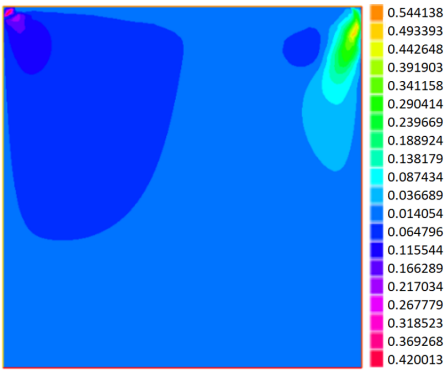

(f) $Re = 1500$

FIGURE 4.3: V-velocity plots for varying values of Re. Other parameters are: $t = 1.5,\ Pr = 5.5,\ Rd = 1,\ Gr_i = 0.0001,\ Gr_v = 0.5$.

As Re increases to 100, inertial effects begin to play a more significant role. The primary vortex shifts upward and becomes more confined toward the upper-left portion of the cavity. Steeper velocity gradients develop near the driven lid and the left boundary, while the lower part of the cavity experiences weaker motion.

Compared with $Re = 1$, the overall V-velocity magnitude decreases, indicating

that momentum transport becomes more localized near the top corners rather than being distributed throughout the domain.

At $Re = 200$, the influence of inertia further strengthens. The main circulation cell is compressed into the upper-left region, and secondary velocity gradients emerge near the right wall. The lower half of the cavity shows relatively stagnant flow. The contours also reveal a noticeable reduction in the maximum V-velocity compared to lower Re cases, indicating that increasing inertia suppresses vertical fluid transport within the cavity.

For $Re = 700$, the V-velocity contours reveal a highly localized circulation region near the upper-left corner. The flow field becomes increasingly asymmetric, with significant velocity concentrated along the top and left boundaries. The central and lower portions of the cavity remain almost motionless, demonstrating that higher inertia strongly restricts vertical velocity transport and confines the motion near the driven boundary. At $Re = 1000$, this trend becomes even more pronounced. The active flow region becomes narrower and remains attached to the lid and the top-left corner of the cavity. The interior domain remains largely stagnant, showing minimal vertical motion. While the maximum V-velocity magnitude is slightly higher than at $Re = 700$, the affected region is smaller, suggesting a stronger concentration of momentum near the lid rather than distributed convection.

Finally, at $Re = 1500$, the flow structure stabilizes and becomes more confined. A single, compact circulation cell persists near the upper boundary, while the rest of the cavity is nearly quiescent. The results highlight the dominance of inertial forces over viscous diffusion at high Reynolds numbers, leading to negligible vertical transport and motion restricted almost entirely to the lid-driven region.

Figure presents with increasing Reynolds number, the flow inside the lid-driven cavity transitions from a simple, viscous-dominated single-vortex pattern to a complex, multi-vortex system. At low Reynolds numbers, a large, central vortex

is the sole feature, but as inertial forces grow, this primary vortex strengthens and shifts its position.

The most significant change is the sequential formation and growth of secondary and tertiary vortices in the corners, driven by flow separation from the stationary walls. This progression demonstrates how increasing fluid inertia leads to a more intricate flow structure with multiple recirculation zones.

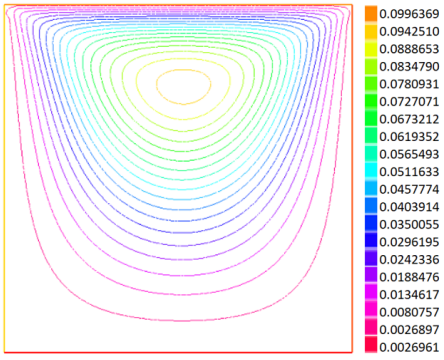

(a) $Re = 10$

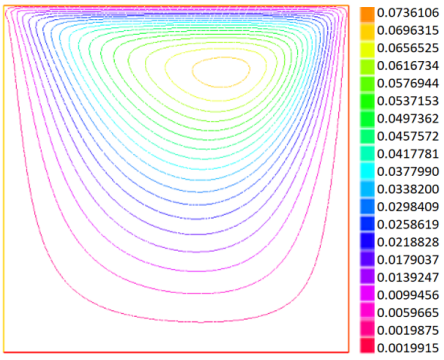

(b) $Re = 100$

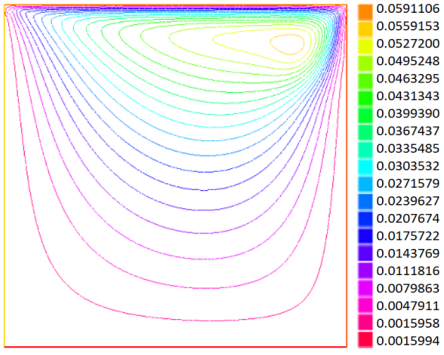

(c) $Re = 200$

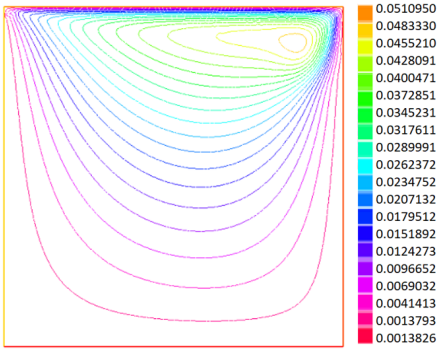

(d) $Re = 300$

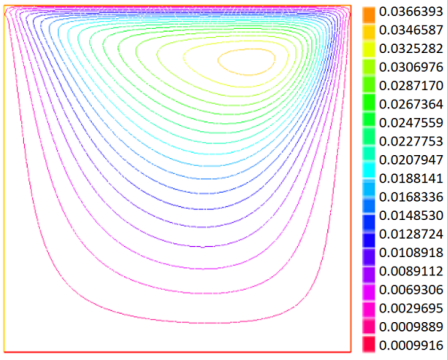

(e) $Re = 700$

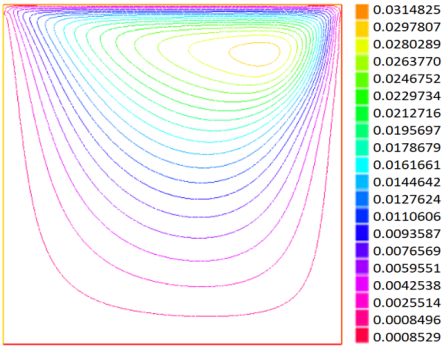

(f) $Re = 1000$

FIGURE 4.4: Streamline plots for varying values of Re. Other parameters are: $t = 1.5,\ Pr = 5.5,\ Rd = 1,\ Gr_i = 0.0001,\ Gr_v = 0.5$.

The figure 4.4 displays the streamlines for the lid-driven cavity at a very low Reynolds number of $Re = 10$. At this Reynolds number, the flow is entirely dominated by viscous forces, resulting in a very predictable and simple flow pattern. The plot shows a single, large, and symmetric primary vortex occupying the majority of the cavity. The streamlines are widely spaced and follow a very smooth path, indicating a weak circulation and a slow, creeping flow. The center of this vortex is located slightly below the geometric center of the cavity, a characteristic feature of lid-driven flow where the viscous drag from the moving lid pulls the vortex downwards.

A key observation is the complete absence of any secondary vortices in the corners. The streamlines gracefully curve along the bottom and side walls without any signs of flow separation or the formation of smaller eddies. This visual evidence clearly confirms that at $Re = 10$, the flow is purely laminar and stable, representing a classic benchmark for the lid-driven cavity problem. This figure shows the streamlines for the lid-driven cavity at a Reynolds number of $Re = 100$.

As the Reynolds number has increased from the previous case, the influence of inertial forces becomes more pronounced, leading to notable changes in the flow pattern. The central primary vortex is still the dominant feature, but it is now visibly stronger. This is evidenced by the streamlines being more concentrated and tightly packed, especially around the core of the vortex. The center of this primary vortex has shifted further downwards and slightly to the right compared to the $Re = 10$ case. This movement is a direct consequence of the stronger inertial forces dragging the fluid along from the top-left to the bottom-right. Despite the increased Reynolds number, the flow remains entirely laminar. There is still no sign of secondary vortices in the corners of the cavity; the streamlines continue to curve smoothly along the stationary walls without forming any closed-loop circulations. This plot represents a transitional stage where the flow is gaining strength and the vortex is shifting, but it has not yet developed the complex features characteristic of higher Reynolds numbers. This figure presents the streamlines for the lid-driven cavity at a Reynolds number of

$Re = 200$. This plot represents a significant turning point in the flow behavior as inertial effects are now sufficiently strong to alter the fundamental flow structure.

The central primary vortex is now much more defined and stronger, as indicated by the very tightly packed streamlines around its core. Its center has shifted to a new, more stable position, slightly downward and centered within the cavity.

The most important development at this Reynolds number is the clear formation of a secondary vortex in the bottom-left corner of the cavity. This is visible as a distinct, closed-loop streamline pattern, which signifies that the main flow is now separating from the bottom wall and creating a counter-rotating eddy.

While smaller, there are also initial signs of a secondary vortex forming in the bottom-right corner. The emergence of these secondary vortices marks the transition from a simple single-vortex flow to a more complex, multi-vortex flow regime, a characteristic progression of the lid-driven cavity problem as the Reynolds number increases.

This figure illustrates the streamlines for the lid-driven cavity at $Re = 300$, where the inertial forces have become even more dominant. The flow structure has become significantly more complex than in the previous cases. The central primary vortex, while still the main feature, has undergone a major transformation. Its core has shifted noticeably upwards and to the right, moving towards the top-right corner of the cavity.

The streamlines are also much more horizontally elongated, showing a stronger, more compressed flow field. Furthermore, the secondary vortices in the bottom-left and bottom-right corners have grown in both size and strength, with their closed-loop streamlines becoming more prominent. A key and crucial development at this Reynolds number is the formation of a tertiary vortex in the top-right corner of the cavity.

This small, distinct closed loop of streamlines is a direct result of the high-velocity flow from the moving lid separating at the stationary corner. The emergence of this third vortex signifies a new level of complexity in the flow field, demonstrating how

increasing Reynolds number progressively alters the flow pattern and generates more intricate recirculation zones.

This figure showcases the streamlines for the lid-driven cavity at $Re = 700$. At this significantly higher Reynolds number, the inertial effects are very dominant, leading to a highly complex multi-vortex flow structure. The central primary vortex is now extremely strong, as evidenced by the very dense and tightly packed streamlines around its core. Its center has shifted again, appearing to move back towards a more central location. The most striking features of this plot are the substantial growth of the secondary and tertiary vortices.

The two secondary vortices in the bottom-left and bottom-right corners have expanded significantly, occupying a much larger area of the bottom part of the cavity. Simultaneously, the tertiary vortex in the top-right corner has also grown considerably and is now a very clear and prominent feature of the flow. The presence and growth of these multiple vortices demonstrate that the increasing inertial forces have led to significant flow separation at all three stationary corners of the cavity. This complex pattern is characteristic of high Reynolds number laminar flow, where the fluid's inertia creates multiple, interconnected recirculation zones.

This figure presents the streamlines for the lid-driven cavity at a high Reynolds number of $Re = 1000$. At this level, inertial forces are highly dominant, and the flow has developed into a complex, multi-vortex system. The central primary vortex remains the main feature, and its core appears to have shifted back towards the geometric center, though it is slightly elongated vertically.

The most striking features are the significant growth and increased strength of all the corner vortices. The two secondary vortices in the bottom-left and bottom-right corners have expanded to occupy a very large portion of the bottom of the cavity. Similarly, the tertiary vortex in the top-right corner has grown considerably and is now a very prominent part of the flow structure. A crucial new development at this Reynolds number is the clear formation of a fourth vortex (a quaternary vortex) in the top-left corner. This small, closed-loop streamline pattern signifies

that the strong inertial flow is now causing separation at all four stationary corners of the cavity.

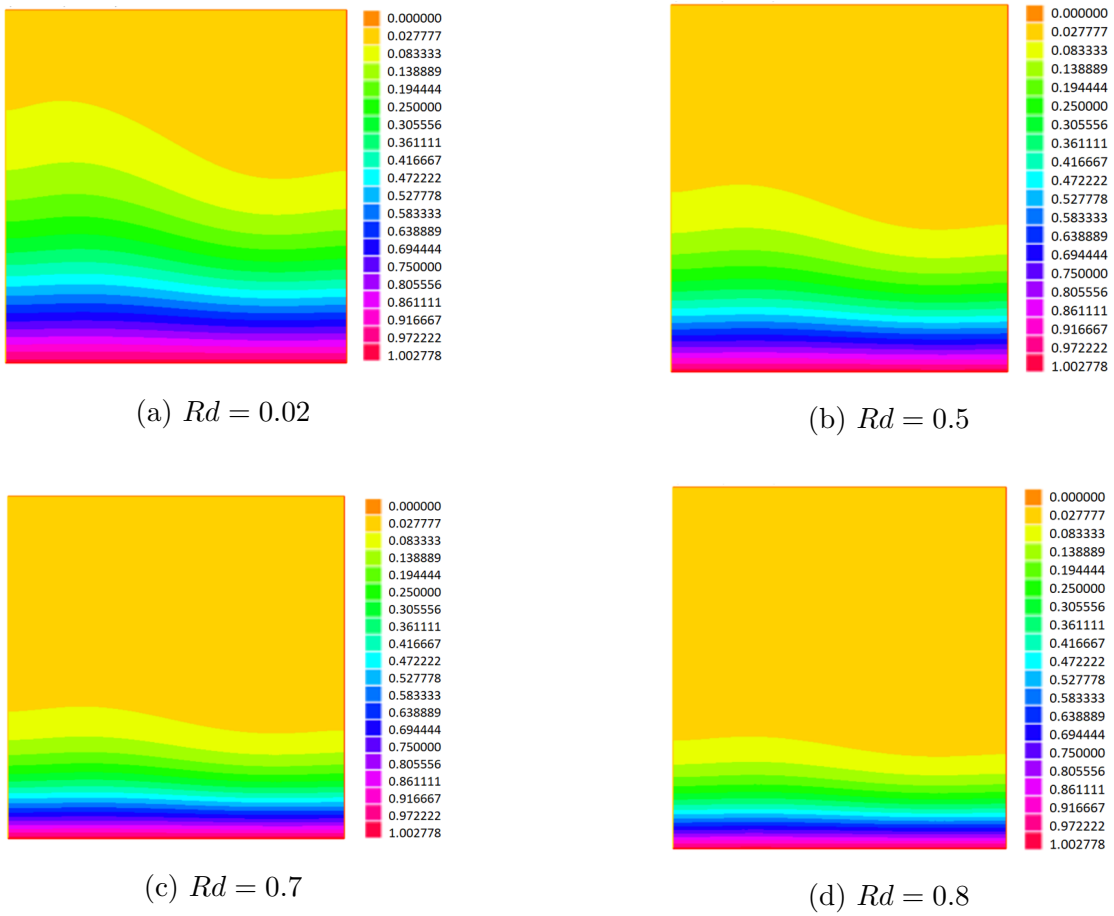

(a) $Rd = 0.02$ (b) $Rd = 0.5$

(c) $Rd = 0.7$ (d) $Rd = 0.8$

FIGURE 4.5: Isotherm plots for varying values of Rd. Other parameters are: $t = 2,\ Re = 50,\ Pr = 1,\ Gr_i = 0.5,\ Gr_v = 0.5$.

Figure 4.5 presents the isotherm plots for different values of the radiation parameter (Rd), with fixed values $t = 2$, $Re = 50$, $Pr = 1$, $Gr_t = 0.5$, and $Gr_p = 0.5$. The radiation parameter characterizes the relative contribution of thermal radiation to heat transfer in the system.

For very small Rd ($Rd = 0.02$), the effect of radiation is weak, and conduction dominates the heat transfer process. The isotherms remain relatively uniform, reflecting limited radiative heat transport. As Rd increases to 0.5, radiative effects become more significant, leading to an enhancement in energy transport away from the surface. This results in more curved isotherms, showing the stronger interaction between conduction and radiation. For higher values ($Rd = 0.7$ and

$Rd = 0.8$), the isotherms are more compressed near the heated surface, indicating that radiation enhances the effective thermal boundary layer thickness. The fluid temperature rises more effectively in the near-wall region, while the outer region remains relatively unaffected. Thus, increasing Rd strengthens radiative heat transfer, enhances the surface heating effect, and modifies the thermal field distribution.

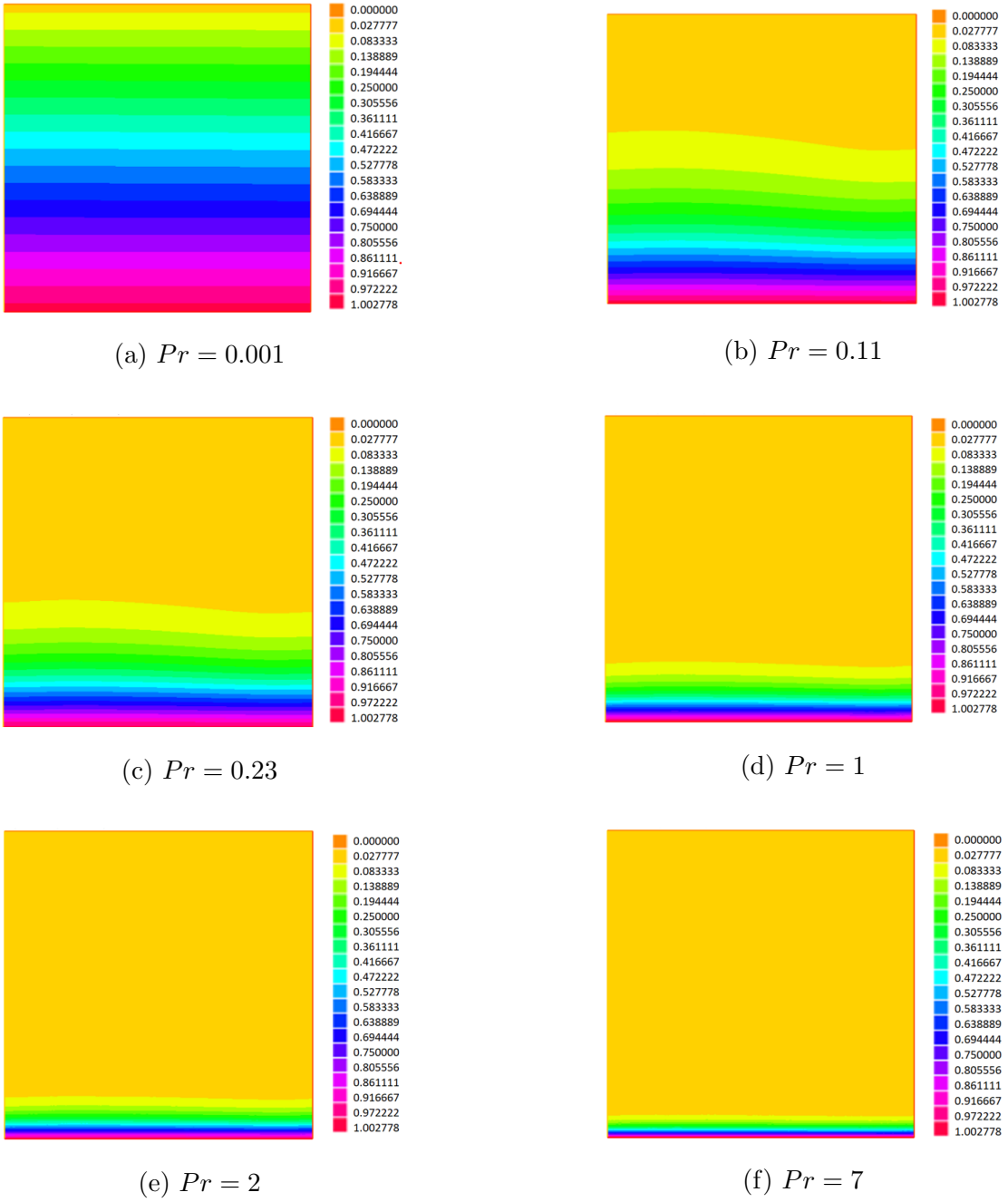

(a) $Pr = 0.001$ (b) $Pr = 0.11$

(c) $Pr = 0.23$ (d) $Pr = 1$

(e) $Pr = 2$ (f) $Pr = 7$

FIGURE 4.6: Isotherm plots for varying values of Pr. Other parameters are: $t = 2,\ Re = 500,\ Rd = 0.1,\ Gr_i = 0.5,\ Gr_v = 0.5$.

Figure 4.6 illustrates the isotherm plots for various values of the Prandtl number (Pr), keeping the other parameters fixed at $t = 2$, $Re = 500$, $Rd = 0.1$, $Gr_t = 0.5$, and $Gr_p = 0.5$. The Prandtl number is the ratio of momentum diffusivity to thermal diffusivity; hence, small values of Pr correspond to fluids with high thermal diffusivity (such as liquid metals), while large Pr values correspond to fluids with relatively low thermal diffusivity (such as oils).

At very low Pr ($Pr = 0.001$), the isotherms are nearly parallel and uniformly distributed, indicating that heat diffuses rapidly throughout the domain. This results in a nearly uniform thermal field, with minimal thermal boundary layer formation.

As Pr increases ($Pr = 0.11$ and $Pr = 0.23$), the isotherms become more compressed near the surface, showing a reduction in thermal diffusion and the development of a stronger temperature gradient close to the boundary.

For moderate values ($Pr = 1$ and $Pr = 2$), a clear thermal boundary layer is observed, with the majority of the temperature variations confined near the surface. This reflects the balance between momentum and thermal diffusion.

At high Pr ($Pr = 7$), the isotherms are tightly packed near the surface, while the rest of the domain remains nearly isothermal. This signifies that heat is strongly restricted to the boundary layer region and does not diffuse far into the bulk fluid. Thus, increasing Pr suppresses the thermal diffusion and enhances the localization of temperature gradients near the surface.

Chapter 5

Conclusion

This thesis carries out a detailed numerical study of two-dimensional incompressible flow and heat transfer within a square cavity filled with a porous medium. The governing relations are formulated using the Darcy–Forchheimer model and include the influence of thermal radiation.

Numerical solutions are obtained through the Finite Element Method (FEM), and the reliability of the implemented code is confirmed by comparison with the benchmark lid-driven cavity results of Ghia *et al.* [31], demonstrating very good agreement.

A detailed parametric study was performed to analyze the influence of the Reynolds number (Re), Prandtl number (Pr), radiation parameter (Rd), and porous medium parameters (Gr_v and Gr_i) on the flow and thermal fields within the cavity.

The key findings of this research are summarized as follows. For low Re, the flow is dominated by viscous effects, resulting in smooth recirculation and symmetric vortex structures. As Re increases, inertia effects become significant, causing the primary vortex to shift toward the upper-left corner and generating stronger secondary vortices near the walls.

At higher Re, fluid motion is largely confined to the lid-driven boundary region. At small Pr values (e.g., liquid metals), thermal diffusion dominates, resulting in nearly uniform temperature profiles. Increasing Pr produces thinner thermal boundary layers near the heated walls, indicating stronger thermal stratification and reduced heat diffusion into the cavity interior. Radiation significantly influences the thermal field. For small Rd, conduction dominates, resulting in smoother and more uniform isotherms.

As Rd increases, radiative effects enhance heat transfer near the walls, causing steeper temperature gradients and more compressed thermal layers. The parameter Gr_v represents viscous resistance, whereas Gr_i corresponds to inertial resistance in the porous medium. Reducing Gr_v (i.e., increasing permeability) leads to stronger convective motion and more pronounced vortex structures. In contrast, Gr_i has a relatively weaker impact at low Re but becomes increasingly significant at higher Re when inertia dominates.

Overall, the results demonstrate that the flow and heat transfer characteristics inside the porous cavity are strongly influenced by the combined effects of radiation, Reynolds number, and Darcy–Forchheimer parameters. At high Re, the motion becomes confined to a thin layer near the moving lid, while increased radiation or reduced permeability leads to sharper thermal gradients and stronger convective currents. In conclusion, this work contributes to a deeper understanding of thermal and flow behavior in porous media under combined Darcy–Forchheimer resistance and radiation effects. The insights gained from this study have potential applications in several engineering fields, including porous heat exchangers, thermal insulation systems, solar collectors, and cooling technologies for electronic devices.

This study lays the groundwork for understanding Darcy–Forchheimer porous cavity flows with thermal radiation. Future research directions may include: investigating three-dimensional unsteady flows to capture transient vortex dynamics and thermal evolution; Studying non-uniform wall heating or variable boundary

conditions for realistic engineering applications; Extending the model to variable porosity or anisotropic porous media.

Bibliography

[1] J. Bear. *"Dynamics of fluids in porous media"*. Courier Corporation, 2013.

[2] K. Vafai. *"Handbook of porous media"*. Crc Press, 2015.

[3] D. A. Nield and A. Bejan. *"Convection in porous media"*. Springer, 2006.

[4] K. Vafai and C. L. Tien. "boundary and inertia effects on flow and heat transfer in porous media". *"International Journal of Heat and Mass Transfer"*, 24 (2):195–203, 1981.

[5] M. Kaviany. *"Principles of heat transfer in porous media"*. Springer Science & Business Media, 2012.

[6] S. Whitaker. *"The method of volume averaging"*. Springer Science & Business Media, 2013.

[7] C. W. Horton and F. T. Rogers Jr. "convection currents in a porous medium". *Journal of Applied Physics*, 16(6):367–370, 1945.

[8] E. R. Lapwood. "convection of a fluid in a porous medium". In *Mathematical proceedings of the cambridge philosophical society*, volume 44, pages 508–521. Cambridge University Press, 1948.

[9] R. A. Wooding. "rayleigh instability of a thermal boundary layer in flow through a porous medium". *Journal of fluid mechanics*, 9(2):183–192, 1960.

[10] A. J. Chamkha. "coupled heat and mass transfer by natural convection about a truncated cone in the presence of magnetic field and radiation effects". *Numerical Heat Transfer: Part A: Applications*, 39(5):511–530, 2001.

[11] P. G. Siddheshwar and U. S. Mahabaleswar. "effects of radiation and heat source on mhd flow of a viscoelastic liquid and heat transfer over a stretching sheet". *International Journal of Non-Linear Mechanics*, 40(6):807–820, 2005.

[12] K. Vafai and C. L. Tien. "combined heat and mass transfer through a porous medium". *International Journal of Heat and Mass Transfer*, 29(7):1099–1112, 1986.

[13] L. C. Chien and C. C. Chen. "analysis of forced convection in a channel filled with a porous medium". *International Journal of Heat and Mass Transfer*, 43(18):3357–3367, 2000.

[14] A. Barletta and E. Magyari. "forchheimer mixed convection in a vertical channel with asymmetric heating". *International Journal of Heat and Mass Transfer*, 50(9–10):1929–1939, 2007.

[15] A. Postelnicu. "influence of magnetic field on heat and mass transfer by natural convection from vertical surfaces in porous media considering soret and dufour effects". *International Journal of Heat and Mass Transfer*, 50 (15–16):3019–3025, 2007.

[16] A. J. Chamkha. "hydromagnetic combined convection flow in a vertical porous channel". *International Journal of Engineering Science*, 40(3):273–287, 2002.

[17] M. A. El-Aziz. "radiation effect on the flow and heat transfer over an unsteady stretching sheet". *International Communications in Heat and Mass Transfer*, 36(5):521–524, 2009.

[18] D. B. Ingham and I. Pop. *"Transport phenomena in porous media III"*, volume 3. Elsevier, 2005.

[19] A. Raptis. "flow of a micropolar fluid past a continuously moving plate by the presence of radiation". *International Journal of Heat and Mass Transfer*, 41(18):2865–2866, 1998.

[20] R. W. Lewis and N. Nithiarasu, P. S. *"Fundamentals of the finite element method for heat and fluid flow"*. John Wiley & Sons, 2004.

[21] W. J. Minkowycz, E. M. Sparrow, G. E. Schneider, and R. H. Pletcher. "handbook of numerical heat transfer". 1988.

[22] F. Hecht. "new development in freefem++". *Journal of numerical mathematics*, 20(3-4):251–266, 2012.

[23] R. K. Bansal. *A textbook of fluid mechanics*. Firewall Media, 2005.

[24] R. K. Rajput. *A textbook of fluid mechanics and hydraulic machines*. S. Chand Publishing, 2004.

[25] J. N. Reddy and D. K. Gartling. *The finite element method in heat transfer and fluid dynamics*. CRC press, 2010.

[26] J. Kunes. *Dimensionless physical quantities in science and engineering*. Elsevier, 2012.

[27] C. P. Kothandaraman. *Fundamentals of heat and mass transfer*. New Age International, 2006.

[28] W. M. Rohsenow, J. P. Hartnett, and Y. I. Cho. *Handbook of heat transfer*, volume 3. Mcgraw-hill New York, 1998.

[29] Yunus Cengel, John Cimbala, and Cengel Cimbala Solutions. Mechanics: Fundamentals and applications cengel... *MECHANICS*, 11:22, 2004.

[30] Purna Chandra Barman, Rishi Raj Kairi, Ashoke Das, and Rabiul Islam. An overview of non-Newtonian fluid. *International Journal of Applied Science and Engineering*, 4(2):97–101, 2016.

[31] K. N. Ghia U. Ghia and C. T. Shin. High-re solutions for incompressible flow using the navier-stokes equations and a multigrid method. *Journal of Computational Physics*, 48(3):387–411, 1982.